

## GENETICS

# Immunity-linked genes are stimulated by a membrane stress pathway linked to Golgi function and the ARF-1 GTPase

Matthew J. Fanelli<sup>1</sup>, Christofer M. Welsh<sup>1,2</sup>, Dominique S. Lui<sup>1</sup>, Lorissa J. Smulan<sup>3</sup>, Amy K. Walker<sup>1\*</sup>

Infection response and other immunity-linked genes (ILGs) were first named in *Caenorhabditis elegans*-based expression after pathogen challenge, but many are also up-regulated when lipid metabolism is perturbed. Why pathogen attack and metabolic changes both increase ILGs is unclear. We find that ILGs are activated when phosphatidylcholine (PC) levels change in membranes of secretory organelles in *C. elegans*. RNAi targeting of the ADP-ribosylation factor *arf-1*, which disrupts the Golgi and secretory function, also activates ILGs. Low PC limits ARF-1 function, suggesting a mechanism for ILG activation via lipid metabolism, as part of a membrane stress response acting outside the ER. RNAi of selected ILGs uncovered defects in the secretion of two GFP reporters and the accumulation of a pathogen-responsive complement C1r/C1s, Uegf, Bmp1 (CUB) domain fusion protein. Our data argue that up-regulation of some ILGs is a coordinated response to changes in trafficking and may act to counteract stress on secretory function.

## INTRODUCTION

Cellular stress responses can react to extrinsic or intrinsic cues and include genes, which counteract effects of stress or support affected cellular functions. Several of the intrinsic stress response pathways are also linked to metabolic processes. For example, overnutrition can lead to metabolic changes that induce cellular stress through an increase in reactive oxygen species (1). Multiple signaling pathways play a dual role, functioning as coordinators of nutrient and stress responses. For example, the nutritional sensor mechanistic Target of Rapamycin (mTORC1) can influence stress-responsive transcription (2). In addition, insulin signaling pathways are strongly linked to stress; mutations in *daf-2*, the *Caenorhabditis elegans* insulin receptor/insulin-like growth factor ortholog, produce highly stress-resistant animals (3). Last, changes in endoplasmic reticulum (ER) lipids have a profound effect on stress pathways (4–6). Specialized ER sensors detect both accumulation of unfolded proteins and overload of the secretory pathway. These sensors then initiate gene expression programs that reduce protein load or increase lipid production (7, 8).

While stress responses and metabolism are intertwined, the biological advantages of linking these processes are less clear. For example, in a previous study, we found that RNA interference (RNAi)-mediated knockdown of two different lipid synthesis modulators, *sams-1* and *sbp-1*, caused up-regulation of pathogen-response genes in *C. elegans*, albeit at a low to moderate level compared to 50- to 100-fold levels during pathogen challenge (9). We also found that *sbp-1*, *sams-1*, and *lpin-1* are part of a feedback loop that responds to shifts in membrane phosphatidylcholine (PC) levels and activates *sbp-1*/SREBP-1-dependent lipogenic programs. This feedback loop is activated in *sams-1* animals when low PC limits cycling of the ARF-1/ARF1 (ADP-ribosylation factor 1)

guanosine triphosphatase (GTPase), altering Golgi dynamics, promoting the proteolytic activation of SBP-1/SREBP-1 and lipid accumulation (9–11). However, despite immune gene up-regulation in basal conditions and constitutive phosphorylation of PMK-1/Mitogen Activated Protein Kinase (MAPK14), an essential immune regulator, *sams-1* animals were sensitive rather than resistant to *Pseudomonas aeruginosa* (PA14). This suggests immunity-linked gene (ILG) activation was not sufficient to confer immunity (9). We noted that while ILG up-regulation after *sams-1* RNAi was only partially dependent on *pmk-1*, restoration of PC levels with dietary choline completely rescued changes in ILG expression and PMK-1 phosphorylation. This suggests that imbalances in membrane lipids may independently affect both the ILG up-regulation and PMK-1 phosphorylation.

The other lipid modulator linked to ILG up-regulation in our previous study was *sbp-1*/SREBPF1, a master transcriptional regulator of lipid synthesis genes (12). It was not clear why the same ILGs would be activated in lipid replete *sams-1* animals because *sbp-1* (RNAi) causes reductions in stored lipids (13, 14). Notably, mammalian SREBPF1 knockdown also results in the enrichment of ILG expression in human cells (15). Recent studies from other laboratories have found that ILGs are up-regulated after mutation or RNAi of genes affecting PC synthesis. ILG activation was seen upon disruption of *pmt-2* (16) or *lpin-1* in the presence of excessive glucose (17). These ILGs were also up-regulated in *skn-1* mutants, a transcriptional regulator of the stress response and metabolic genes (18). In addition, dietary restriction results in the up-regulation of similar gene sets (19). These results suggest that multiple lipid imbalances affect ILG expression, and some mechanisms may be conserved. Immunity-linked categories are enriched in up-regulated genes after SREBP-1 knockdown in human melanoma cell lines (15). These results suggest that ILG up-regulation in *sams-1* or *sbp-1* (RNAi) animals could occur with different kinetics and in response to distinct cues than their activation in classical pathogen responses.

Exposure of *C. elegans* to bacterial pathogens stimulates the expression of a diverse set of genes, including antimicrobial peptides

<sup>1</sup>Program in Molecular Medicine, UMASS Chan Medical School, Worcester, MA, USA. <sup>2</sup>Morningside School of Biomedical Sciences, UMASS Chan Medical School, Worcester, MA, USA. <sup>3</sup>Department of Medicine, UMASS Chan Medical School, Worcester, MA, USA.

\*Corresponding author. Email: amy.walker@umassmed.edu

(AMPs), enzymes for detoxifying xenobiotics, and neuromodulatory peptides to coordinate interorgan defenses (20–23). However, some genes up-regulated in response to either bacteria or fungi do not fall into these defensive pathways (24) or have clear functional roles. Instead, these genes are defined by pathogen-responsive expression rather than the performance of a function during the pathogen response. Because of the effects on these genes by a broad number of lipid perturbations and the modest levels of up-regulation compared to pathogen-stimulated responses, we reasoned that some of these genes responding to cell-intrinsic signals independent of the pathogen response. To understand why the knockdown of genes acting in lipid metabolism might activate genes linked to immune responses when no pathogens were present, we took two approaches. First, we looked for lipid signatures that could signal this response and were shared between *sams-1* and *sbp-1* by comparing lipidomics of whole animals and fractionated extracts. Second, we performed an RNAi screen of genes functioning in complex lipid synthesis and ER/Golgi dynamics for activation of the immunity-linked reporter, *psysm-1::GFP* (25). In the lipidomics studies, we found that *sams-1* and *sbp-1* knockdown animals had broad and distinct changes in their lipidome, but both showed a lowering of PC levels in the ER/Golgi fraction, which we previously linked to SBP-1/SREBP-1 maturation in *sams-1* animals (10). Strengthening the links to PC, our targeted RNAi screen showed that synthesis of PC increased *psysm-1::GFP* expression. RNAi of Golgi/ER transport regulators, including the GTPase *arf-1/ARF1*, activated the immunity-linked reporter. Notably, some ILGs were up-regulated after *arf-1/ARF1* RNAi, demonstrating that this disruption in this secretory organelle was sufficient to activate ILGs. We also noted that overexpression of secreted proteins causes a dose-dependent increase in ILG expression in published RNA sequencing (RNA-seq) data. Last, we performed a targeted screen and found that interfering with ILG expression in *sbp-1(ep79)* animals disrupted the trafficking of a secreted reporters in two distinct tissues. Together, our results suggest that some ILGs act to counteract stress when membrane lipid balance is perturbed or when other processes, such as antimicrobial production, affect secretory load. While immune function is critical for host defenses, immune activation in the absence of pathogens, as in the case of metabolic disease, may have deleterious effects (26). Therefore, it is critical to understand roles of genes activated in response to both pathogens and metabolic cues. Our studies suggest that genes stimulated by both bacterial challenge and lipid perturbation in *C. elegans* could act to support secretory processes, which are altered in both biological contexts.

## RESULTS

### Meta-analysis illustrates broad enrichment of ILGs upon disruption in lipid metabolism

Levels of lipids within membranes are tightly monitored, and imbalances may induce cellular stress pathways that regulate genes to restore lipid ratios (7). ILG activation has been reported to occur in multiple lipid perturbation models, suggesting that it could be part of a general membrane stress response. To determine how broad this effect might be and identify specific classes of pathogen-responsive genes, we used our recently developed *C. elegans*-specific Gene Ontology (GO) tool, WormCat 2.0, to conduct a meta-analysis of genes activated after disruption of lipid

metabolism. WormCat allows combinatorial graphing of gene enrichment scores based on detailed annotation of all *C. elegans* genes (27, 28) and uses a custom annotation strategy based on broad to specific nested categories (CATEGORY1/Category2/Category3). Unlike GO, it assigns genes with poorly defined functions to a specialized category, UNASSIGNED. Unassigned is also used within categories when genes are linked to a category but do not have well-defined molecular roles. In WormCat, genes with roles in immunity are classified in STRESS RESPONSE: Pathogen at the category 1 and category 2 levels. This category is broken down into category 3 classifications for transcriptional or signaling regulators, neuropeptide-like proteins, and proteins containing common antimicrobial motifs [saposin, caenacin, complement C1r/C1s, Uegf, Bmp1 (CUB), and others]. This category also included 97 additional genes that are robustly activated during pathogen responses. These genes did not have essential roles in survival or defined molecular functions yet are commonly used as proxies for immune stimulation. These genes were placed in STRESS RESPONSE: Pathogen: *unassigned* (27, 28). This class of genes is not explicitly defined by GO but can be differentiated with WormCat. We performed a meta-analysis using WormCat to compare published RNA-seq data from models of disrupted lipogenesis with genes up-regulated by the pathogen PA14 (23). Consistent with other reports, this analysis shows enrichment in STRESS RESPONSE: Pathogen in genes up-regulated after the knockdown of lipogenic transcriptional regulators such as *sbp-1* (9), *mdt-15* (29), or *nhr-49* (30) or enzymes acting in lipid synthesis such as *sams-1* (9), *lpin-1* [(17) and data S1], *pmt-2* (6), and *hyl-2* (31). Similar enrichment patterns occur when exogenous lipids such as P80 (oleic acid mimic) (32) or cholesterol were added (33) (Fig. 1, A to D). Notably, the strongest enrichments at the category 3 level were in STRESS RESPONSE: Pathogen: *unassigned*, and lipid disruption had a much weaker effect on other classes of pathogen response genes, such as the CUB domain proteins, which are likely to act as antimicrobials. Genes up-regulated in *pmt-2(RNAi)* animals were also linked to the lipid bilayer stress-induced unfolded protein response (UPR<sup>LS</sup>), a UPR<sup>ER</sup> mechanism (6). Therefore, we compared WormCat enrichment of genes increasing after tunicamycin treatment to determine whether ILG up-regulation after lipid perturbation was similar to an ER stress response (34). We found that while STRESS RESPONSE: Pathogen: *unassigned* genes were enriched, the category enrichment was independent of the ER stress regulators *xbp-1* or *ire-1* (fig. S1A), suggesting that the ILG up-regulation could have distinct regulatory elements from the UPR<sup>ER</sup>. Thus, genes linked to immunity are up-regulated across diverse lipid synthesis modulators in *C. elegans* and mammalian cells.

### *sams-1* and *sbp-1* are likely to act independently to activate ILGs

Our previous studies low levels of PC initiate a feedback loop in *sams-1* animals driving SBP-1/SREBP-1-dependent lipid accumulation (9, 11). SBP-1/SREBP-1 is a basic helix-loop-helix transcription factor required to express a suite of lipid metabolic genes, including *fat-7* in *C. elegans* and its ortholog SCD1 in mammals (14, 35). It is also necessary for the up-regulation of *fat-7* in lipid-replete *sams-1(lof)* animals (fig. S1D) (11). Because SBP-1 up-regulates lipid synthesis genes, we tested the possibility that it directly functions in ILG up-regulation by using *sams-1(RNAi)* to increase the expression of multiple SBP-1 target genes (11) and assessing the

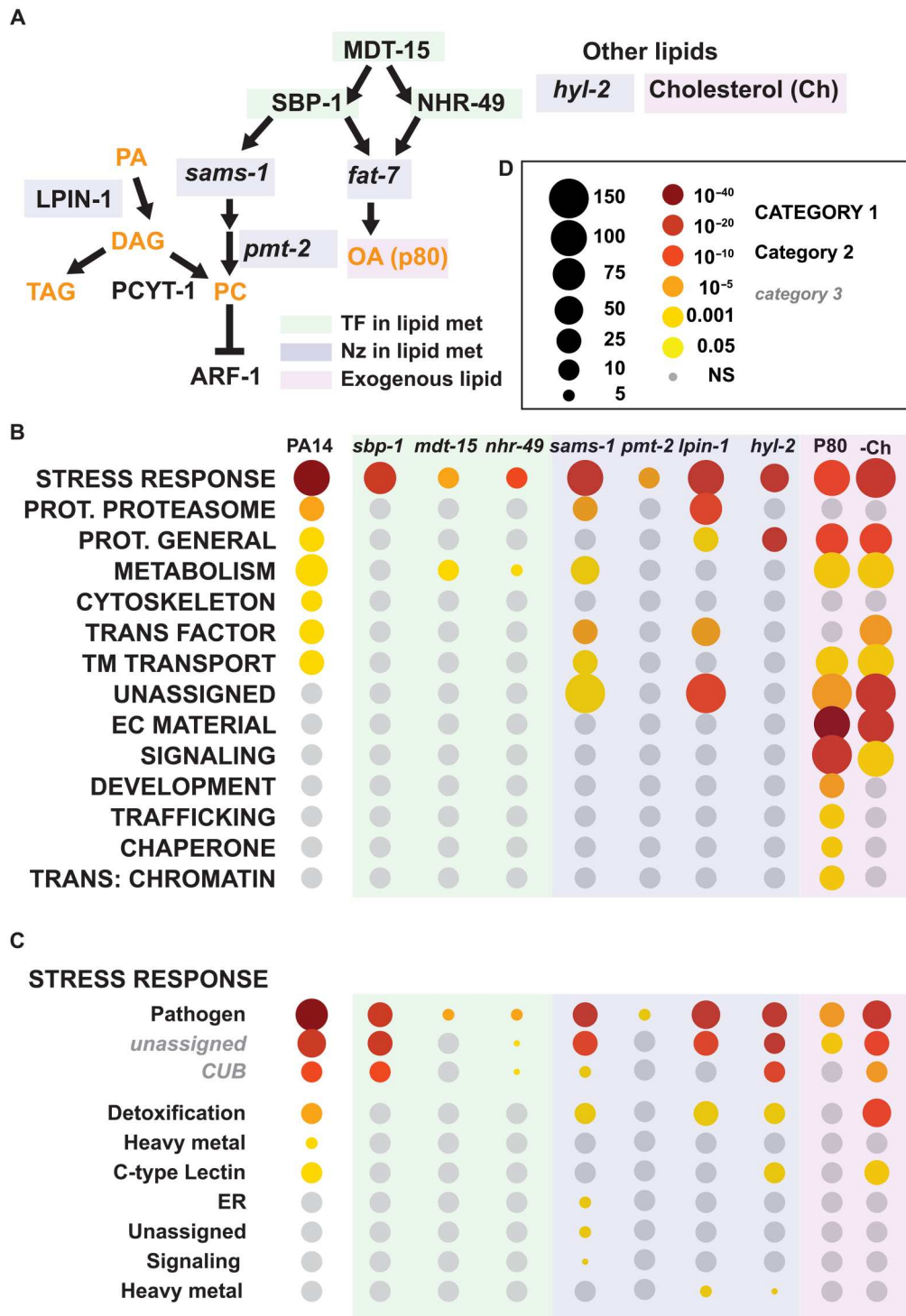


**Fig. 1. Up-regulation of ILGs occurs downstream of multiple types of membrane lipid disruption.** (A) Schematic diagram of lipid metabolic genes linked to immune gene expression. Meta-analysis of published RNA-seq data from linking lipid perturbation to immune gene expression using WormCat 2.0 for category 1 (B) and for the category 2 level under STRESS RESPONSE (C). Legend is in (D). NS, not significant.

need for *sbp-1*. As we previously reported in (11), *fat-7* depends on *sbp-1* in both the control and *sams-1(RNAi)* background (fig. S1D). However, the ILG *hpo-6* is expressed at high levels when induced by reduction in *sbp-1*, *sams-1*, or in *sams-1(lof)*; *sbp-1(RNAi)* animals (fig. S1E), suggesting that the effects of SBP-1 on ILG up-regulation are indirectly related to its function as a transcriptional regulator. These results also suggest that *sams-1* and *sbp-1* are not likely to act on each other in ILG up-regulation but could be linked to similar cues.

Many ILGs in *C. elegans* act downstream of signals from the p38/MAPK14 kinase PMK-1 in the pathogen response (23), although PMK-1 may also act in other stress responses (36–39). In previous studies, we found that low PC in *sams-1(lof)* animals leads to constitutive phosphorylation of PMK-1 and that ILG induction is completely dependent on PC (9). However, the up-regulation of ILGs in *sams-1(RNAi)* animals was only partly dependent on *pmk-1* (9), suggesting that perturbations in membrane lipids could activate these genes through distinct pathways. We confirmed that knockdown of *sbp-1* also induces PMK-1 phosphorylation (fig. S1F). Because ILGs can be induced in mammalian cells in response to a reduction in *SREBF1*, we used small interfering RNA (siRNA) to knock down the rate-limiting enzyme for PC production, *PCYT1*, in human hepatoma cells (fig. S1G). We found that p38/MAPK14 phosphorylation is induced to levels similar to lipopolysaccharide. However, as in the case of *sams-1(RNAi)*, quantitative reverse transcription polymerase chain reaction (qRT-PCR) assays show that induction of ILGs in *sbp-1(RNAi)* animals was only partially dependent on *pmk-1* (fig. S1H). This suggests the low-moderate levels of ILG activation in response to membrane lipid imbalances could depend on distinct mechanisms from those used to induce these genes during pathogen responses.

### Loss of *sbp-1* decreases PC levels in ER/Golgi membrane fractions

ILG expression and PMK-1 phosphorylation occur after reduction in *sams-1* and *sbp-1*, although these genes act at different points in regulation of lipid synthesis. SAMS-1 provides S-adenosylmethionine (SAM), the methyl donor necessary for one of the two pathways for PC production. However, as the master transcriptional regulator of lipid biosynthetic genes, *sbp-1/SREBF1* would be predicted to affect a broad fraction of the lipidome, and it is not clear how *sams-1* and *sbp-1* lipidomes would overlap. To allow a direct comparison of lipidomes, we performed *sbp-1* and *sams-1 RNAi* and directly compared lipidomes by liquid chromatography–mass spectrometry (LC-MS). Animals were lysed directly into the lipid extraction buffer, and lipid levels were normalized to total lipid as in (10). The entire lipidome was broadly altered in both cases, with 27% of lipid species showing statistically significant changes in *sams-1(RNAi)* animals and 30% after *sbp-1(RNAi)* (Fig. 2, A and B, and data S2). We next examined lipid levels at the class and species levels. As in our previous gas chromatography–mass spectrometry–based studies (11), *sams-1* animals showed lower PC and higher triglyceride (TAG) (Fig. 2C). We also noted lower phosphatidylserine and sphingomyelin (SM) levels in comparison to other lipid classes (fig. S2A). TAG was lower after *sbp-1 RNAi*, as expected from previous studies (13). We also found that while reductions in PC did not reach statistical significance, phosphatidylethanolamine (PE) increased, and Cer (Ceramide) levels dropped (fig. S2A). In short, *sbp-1 RNAi*

induces broad changes in the lipidome across multiple classes of lipids, with the largest changes in stored lipids, TAGs.

The properties of lipid classes can be altered when distributions of acyl chains alter membrane properties (40). We find that there are significant differences in the populations of species within phospholipids [PC, PE, lyso-phosphatidylethanolamine, and phosphatidylglycerol, TAG, diacylglycerides (DGs), and SMs after *sams-1 (RNAi)*. Changes in species distribution in lipid classes after *sbp-1 RNAi* were limited to TAG, lyso-PC, and Cer, in agreement with previous studies showing lower TAGs in *sbp-1(RNAi)* animals. We asked if *sams-1* and *sbp-1 RNAi* caused similar shifts and found overlapping changes in 180 shared lipid species (data S2). Comparison of lipids within each class that increased or decreased with *sams-1* or *sbp-1 RNAi* shows little overlap in the major lipid classes of TAG, PE, and DG (Fig. 2, D to H; fig. S2, C and D; and data S2). However, nearly half of PC species decreasing after *sbp-1* knockdown also decreased in *sams-1(RNAi)* animals (Fig. 2I). Last, three SM species decreased in both animals (fig. S2A). Thus, while *sams-1* or *sbp-1* knockdown each lead to broad changes in the total lipidome, relatively few overlapping species changed in both instances. Of those, decreases in PC species were the best represented among lipids changed in both *sams-1* or *sbp-1* animals.

The total lipidome contains multiple organelles, including the plasma membrane, mitochondria, nuclear membrane, and Golgi/ER. However, lipid ratios in specific organelles may differ, reflecting particular functions (41); for example, we previously found that PC ratios in ER/Golgi fractions were associated with the activation of SBP-1 in *sams-1* and *lpin-1* animals (10). Therefore, we performed LC-MS lipidomics on microsomes from *sbp-1(RNAi)* animals to assess lipids in the ER/Golgi fraction using total protein for normalization. Enrichment of Golgi and ER-specific proteins [SQV-8 and CNX-1 (42)] was used to verify fractionation, as in our previous study (10) (fig. S2C). We found that a broader fraction of the ER/Golgi lipidome was affected after *sbp-1(RNAi)* than in the total lipid samples. Nearly 40% of lipid species were altered in these fractions (Fig. 2J and data S2), with significant changes in species across many classes (fig. S2K and F and G). Similar to the unfractionated extracts, levels of TAG and Cer decreased in the ER/Golgi (fig. S2F). Significant ER/Golgi-specific decreases occurred in PC and DG (Fig. 2F and fig. S2E). This reveals that *sbp-1(RNAi)* has distinct effects on the ER/Golgi membranes compared to the total lipidome. It also demonstrates decreases in PC levels in the ER/Golgi subcompartment after *sbp-1* knockdown, which is also strongly affected after *sams-1 RNAi*.

### Targeted RNAi screen reveals roles for COP I transport in immune gene expression

Low PC levels are associated with ILG expression in *sams-1* (9) and *pmt-2(RNAi)* animals (6). The low PC in the ER/Golgi compartment of both *sams-1* (10) and *sbp-1 RNAi* animals suggests that this could be a shared signature linked to ILG up-regulation. To understand how these lipids might act, we next sought to identify cellular pathways linking ILG expression to lipid levels. We used an RNAi sublibrary that targets genes involved in complex lipid metabolism, lipid signaling, and selected ER/Golgi transport regulators. We previously used a lipid function RNAi sublibrary to identify low PC regulators of SBP-1/SREBP-1 (10). This library includes all predicted phospholipases and enzymes for the synthesis of TAG, PC, and PE (10). We expanded the sublibrary to include

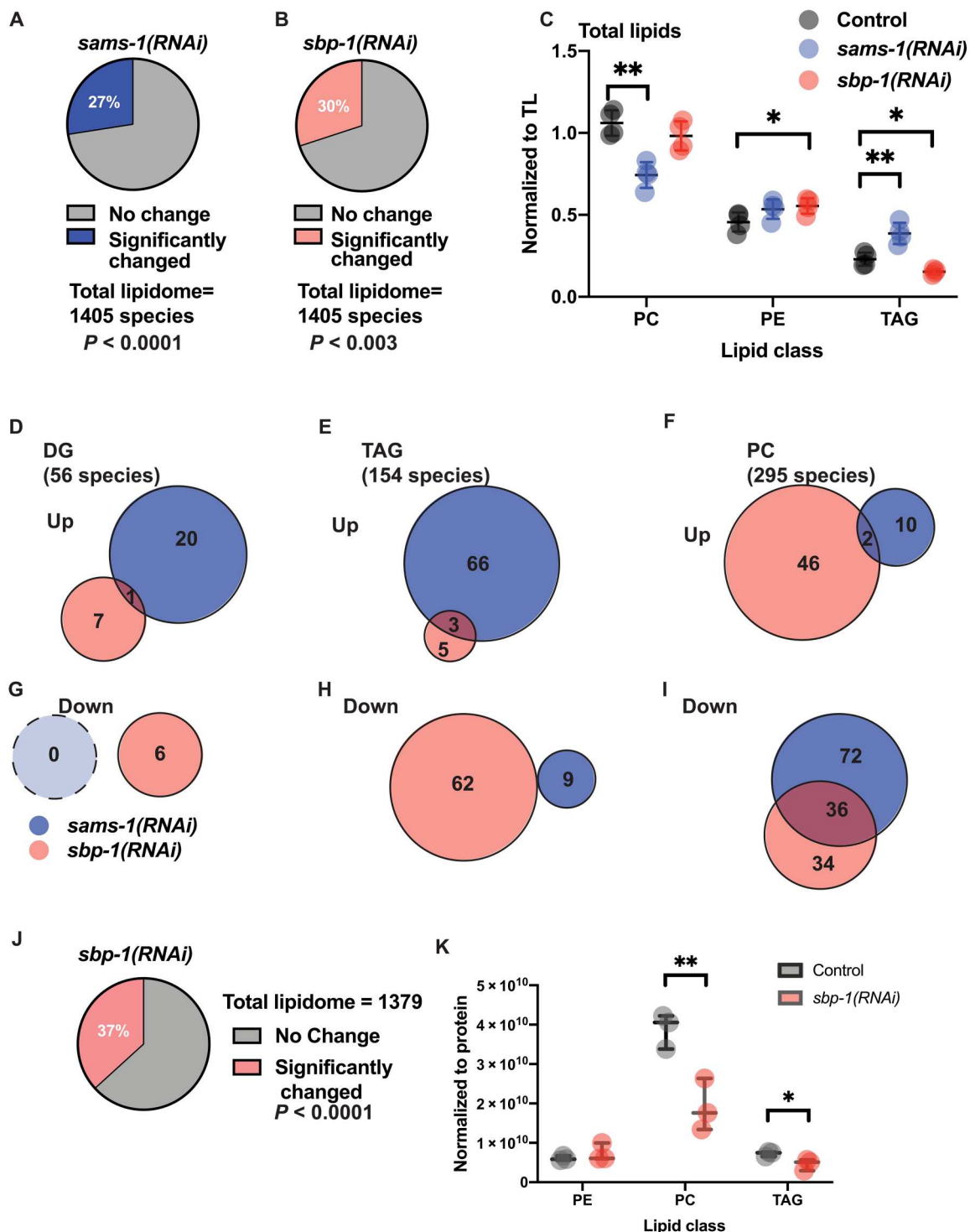


**Fig. 2. Broad lipidomic changes in total and microsomal lipid compartments after *sams-1* or *sbp-1* RNAi.** LC-MS lipidomics show that nearly a third of total lipid species change after *sams-1* or *sbp-1* RNAi (A and B). Comparison of total lipid levels within major classes does not reveal a similar, significant signature after *sams-1* or *sbp-1* RNAi (C). See also fig. S1 (B and D) additional lipid class analysis and data S2 for all values. Overlap in lipid species that significantly changed from classes that significantly changed after *sams-1* or *sbp-1* RNAi are compared in Venn diagrams. Species that increased are shown in (D to F), with decreases in (G to I) with additional lipids in fig. S2C. The microsomal (ER/Golgi) lipidome is also broadly altered after *sbp-1* RNAi (J) and shows changes in different lipid classes than in the total lipidome (K). See also fig. S1 (E and F) additional lipid class analysis and data S2 for all values. Error bars show SD. Lipid class data are calculated by Student's *t* test. See fig. S1 for lipid species distributions and additional lipid class analysis. \* $P < 0.05$  and \*\* $P < 0.01$ . DG, diacylglyceride; TAG, triglyceride; PC, phosphatidylcholine; PE, phosphatidylethanolamine; TL, total lipid.

more genes involved in ceramide/SM synthesis for the current screen. Thus, this library has a broader representation of genes linked to complex lipid synthesis than the commercially available RNAi libraries. We selected *psysm-1::GFP* (green fluorescent

protein) for this study as it is strongly induced by *sbp-1(RNAi)* (Fig. 3A) and has been used by multiple laboratories as a robust marker for immune gene induction (19, 43, 44). We visually screened this library in quadruplicate in *psysm-1::GFP* animals,

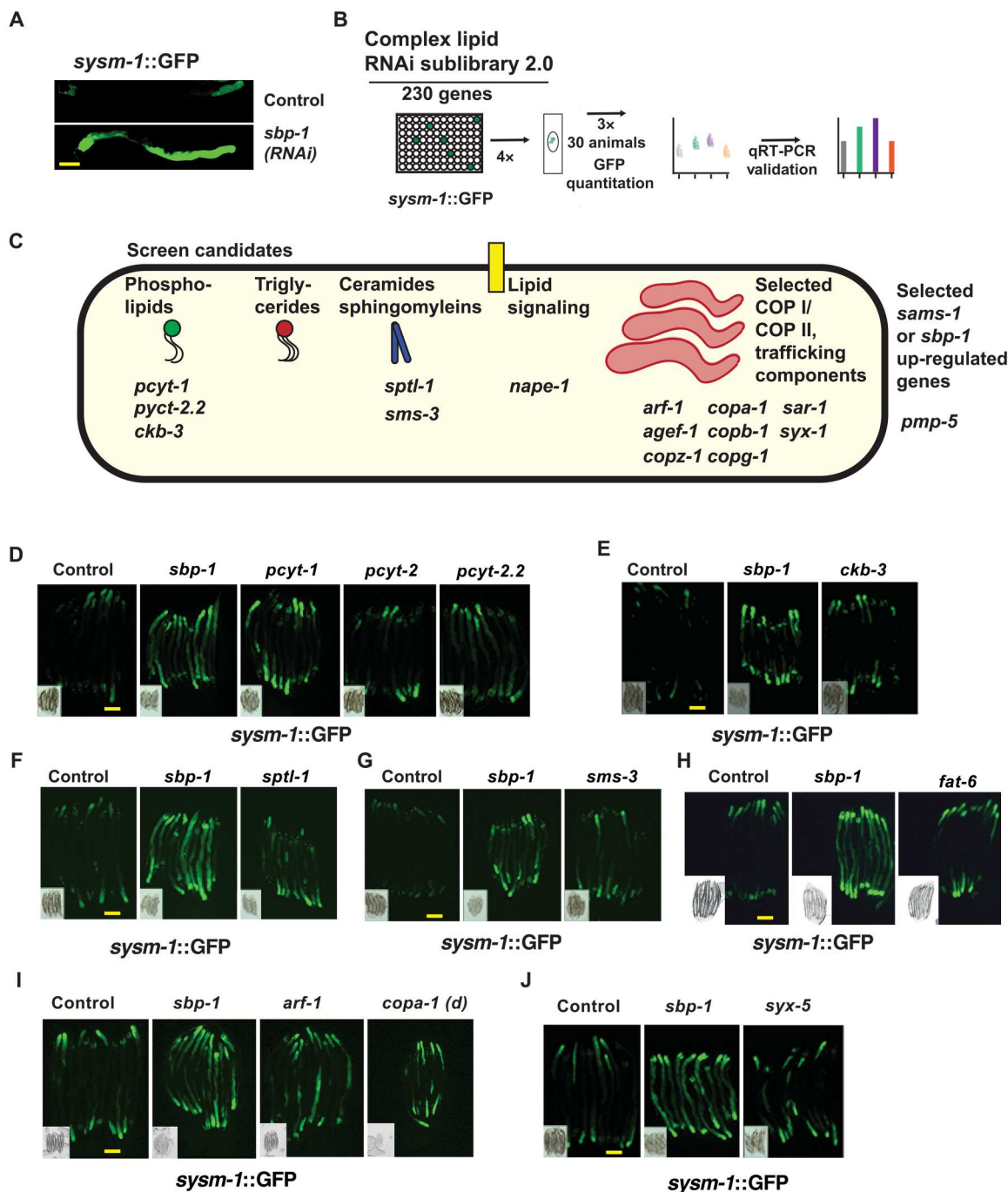


**Fig. 3. Targeted RNAi screen reveals candidates linked to Golgi/ER trafficking impact immunity gene expression.** (A) Immune gene reporter *psysm-1::GFP* is increased after *sbp-1* RNAi. (B) Screen schematic. (C) Schematic showing candidates from primary screen selected for additional quantitation. Example epifluorescence imaging used for quantitation showing validation of reporter activity after RNAi of lipid PC synthesis genes (D and E), SM synthesis genes (F and G), and the SCD *fat-6/7* (H). Epifluorescence images showing GFP levels after RNAi of the *arf-1* GTPase or coatomer component *copa-1* or proteins acting at the Golgi such as *syx-1*/Syntaxin5 (I and J). Because of poor larval development, bacteria for *copa-1* RNAi was diluted to 1:10 (d). Internal control for effect of *sbp-1(RNAi)* included in each panel and differential interference contrast (DIC) image included as an inset for each RNAi. Quantitation of images is in fig. S4 (A and B). Scale bars, 100  $\mu$ m.

scoring each animal, and identified a list of 20 candidates with the highest aggregate scores for retesting (Fig. 3B and data S3). Retesting to identify the strongest candidates occurred in three stages: visual rescreening (4×), imaging of candidates from the rescreen, and qRT-PCR to assess changes in GFP expression. We also included the *sbp-1* target genes *fat-5*, *fat-6*, and *fat-7* (13, 14) in the visual retesting. These genes are orthologs of mammalian stearyl CoA desaturases (SCDs) (45) and can change membrane fluidity (46, 47) or induce lipid bilayer stress by changing ratios of saturated/unsaturated acyl chains within lipid classes (6, 16, 48).

Candidates from the targeted screen fell into two major groups. First, enzymes linked to PC and SM synthesis were found (Fig. 3, C to G; fig. S3, A and B; and data S3). This included two isoforms of the rate-limiting enzyme for PC production, *pcyt-1* and *sptl-1*, which initiates the first committed step in sphingolipid synthesis. Thus, our genetic data support the notion that changes in PC or SMs are a shared signature linked to ILG activation in *sams-1* and *sbp-1* RNAi animals. SM synthesis has been linked to multiple stress responses in *C. elegans* (49–51). Notably, *fat-5*, *fat-6*, or *fat-7* RNAi, which would change acyl chain saturation within each lipid class, had modest effects on the *psysm-1::GFP* immune reporter in quantitation of fluorescence images (data S3), suggesting that change in membrane fluidity downstream of these enzymes in the UPR<sup>LBS</sup> (6, 16) is not a major contributor to the ILG up-regulation.

The second group included Golgi/ER trafficking genes forming the Coat Protein 1 (COP1) complex (which also caused developmental delays) and ARF1 guanine activating factor (*agef-1*). The ARF-1 GTPase, a key regulator of these factors, was a false negative in the original screen but strongly activated the reporter in the rescreening (Fig. 3I and data S3). The coatmer proteins work in a complex (52) and are required for viability (53). Therefore, we chose one candidate, *copa-1*, and performed RNAi with diluted bacteria (d), allowing animals to develop fully. We found that the immune activation reporter was strongly expressed in the *copa-1* knockdown (Fig. 3I). Stimulation of the reporter after the loss of multiple parts of the COP I machinery and its key regulator *arf-1* strongly argues that ER/Golgi dynamics signal to induce ILGs. The *psysm-1::GFP* reporter represents a single gene in the immune response program. To more broadly survey ILGs in our screen validation, we used qRT-PCR with primers specific to *irg-1*, *irg-2*, and *hpo-6* and found robust activation of our candidate reporters after knockdown of *arf-1* or *copa-1* but more modest effects with the SM genes or SCDs (fig. S4, C to H), implicating ARF1 and Golgi function in ILG activation. Although *syx-5* appeared in our initial screen, GFP levels were not significantly changed after image quantitation (Fig. 3J).

### Reduction in ARF-1 has a broad effect on ILGs

Cycling of the ARF1 GTPase requires interaction with the Golgi membrane (52). Alteration of membrane lipid ratios can affect interactions with ARF1 regulatory proteins, limiting GTPase cycling and blocking ARF1 activity (10, 54). We previously linked changes in PC levels in *sams-1* microsomes to the inactivation of ARF-1, which drove proteolytic processing of SBP-1/SREBP-1 (10). Therefore, we reasoned that this PC-ARF-1 mechanism could also be important in activating ILGs. To test this, we use RNA-seq to identify transcriptional changes after *arf-1* RNAi. We found that 210 genes were significantly up-regulated after *arf-1* RNAi (Fig. 4A and data S4). STRESS RESPONSE: Pathogen: *unassigned* was significantly

enriched, demonstrating that interference with *arf-1* is sufficient to induce this gene class (Fig. 4B). We also noted strong overlap between genes up-regulated in *sams-1*, *sbp-1*, and *arf-1* (Fig. 4C). This overlap set retains the significant enrichment in STRESS RESPONSE: Pathogen: *unassigned* genes (Fig. 4D). Thus, *arf-1* GTPase knockdown causes similar or overlapping effects in immune gene expression to those seen after broad lipid disruption by *sbp-1* RNAi. Together with our previous observation that low PC disrupted ARF-1 function (10), our data suggest that changes in ARF-1 activity could provide the mechanistic link between PC and activation of ILGs in some models of membrane lipid imbalance.

To test this model by examining ARF-1 localization, we obtained a strain where endogenous ARF-1 is C-terminally tagged with mCherry by CRISPR. This strain was crossed with a strain expressing MANS::GFP in the intestine. MANS::GFP is a fusion of *aman-2* (alpha-mannosidase, a conserved Golgi-specific protein) and marks the mini stacks characteristic of *C. elegans* (55). In control intestinal cells, ARF-1::mCherry formed a punctate pattern (Fig. 4E) characteristic of the Golgi ministacks occurring in *C. elegans* cells (56) and which overlap a Golgi marker, MANS::GFP (57). This suggests that, as in other eukaryotes, *C. elegans* ARF-1 acts at the Golgi apparatus. Next, we asked if ARF-1 localization was altered in *sbp-1*(RNAi) animals. Strikingly, ARF-1::mCherry appeared to form larger, more irregular puncta in *sbp-1*(RNAi) animals and having additional diffuse localization, similar to patterns seen with RNAi of the coatmer protein COPA-1 (Fig. 4F). This suggests that ARF-1 functions at the Golgi are altered in *sbp-1*(RNAi) animals.

Loss of human ARF1 or blocking ARF1 cycling with the fungal toxin Brefeldin A disrupts Golgi integrity (58). In addition, our previous studies found that lowering PC levels through RNAi of *sams-1* or knockdown of *PCYT1* (the rate-limiting enzyme for PC production) in mammalian cells blocked ARF1 GTPase activity and disrupted Golgi structure (10, 11). Because PC levels in *sbp-1*(RNAi) ER/Golgi fractions decreased (Fig. 2K) and ARF-1::mCherry was mislocalized, we next examined Golgi structure after *sbp-1*(RNAi) in animals where MANS::GFP was driven by an intestinal reporter (57). Consistent with previous studies (59, 60), the knockdown of *arf-1* markedly shifts the Golgi puncta to diffuse localization across the cytoplasm (Fig. 4G and fig. S4D). *copa-1* RNAi also diminished Golgi stacks. *Sbp-1* knockdown affects Golgi structure but results in a different pattern, in which Golgi stacks are smaller and more numerous with increases in diffuse cytoplasmic localization (Fig. 4G). This suggests that membrane lipid imbalances affect the Golgi size or structure but do not disassemble it. We also examined MANS::GFP patterns in other candidates from our screen and noted that like *arf-1*, *copa-1* and *sar-1* were also required for MANS-1::GFP puncta (fig. S4A), as expected for a core constituent of the ER to Golgi transport machinery. Contributors to PC synthesis also broadly abrogated MANS::GFP puncta (fig. S4, B and C). However, the change in fatty acid desaturation, which induces UPR<sup>LBS</sup> (6), caused only a slight increase in MANS::GFP puncta intensity, suggesting that membrane stress initiated by Golgi misfunction has separable defects. Our screen candidates also included genes from ceramide synthesis, which can also affect membrane function (61). Notably, *sptl-1*(RNAi) did not noticeably alter Golgi marked by MANS::GFP, and ARF-1::mCherry puncta were visible (fig. S4, A and D), suggesting that *sptl-1* knockdown may mediate effects on immune genes through distinct cellular membranes. Together, we find ARF-1 activity (10) and localization

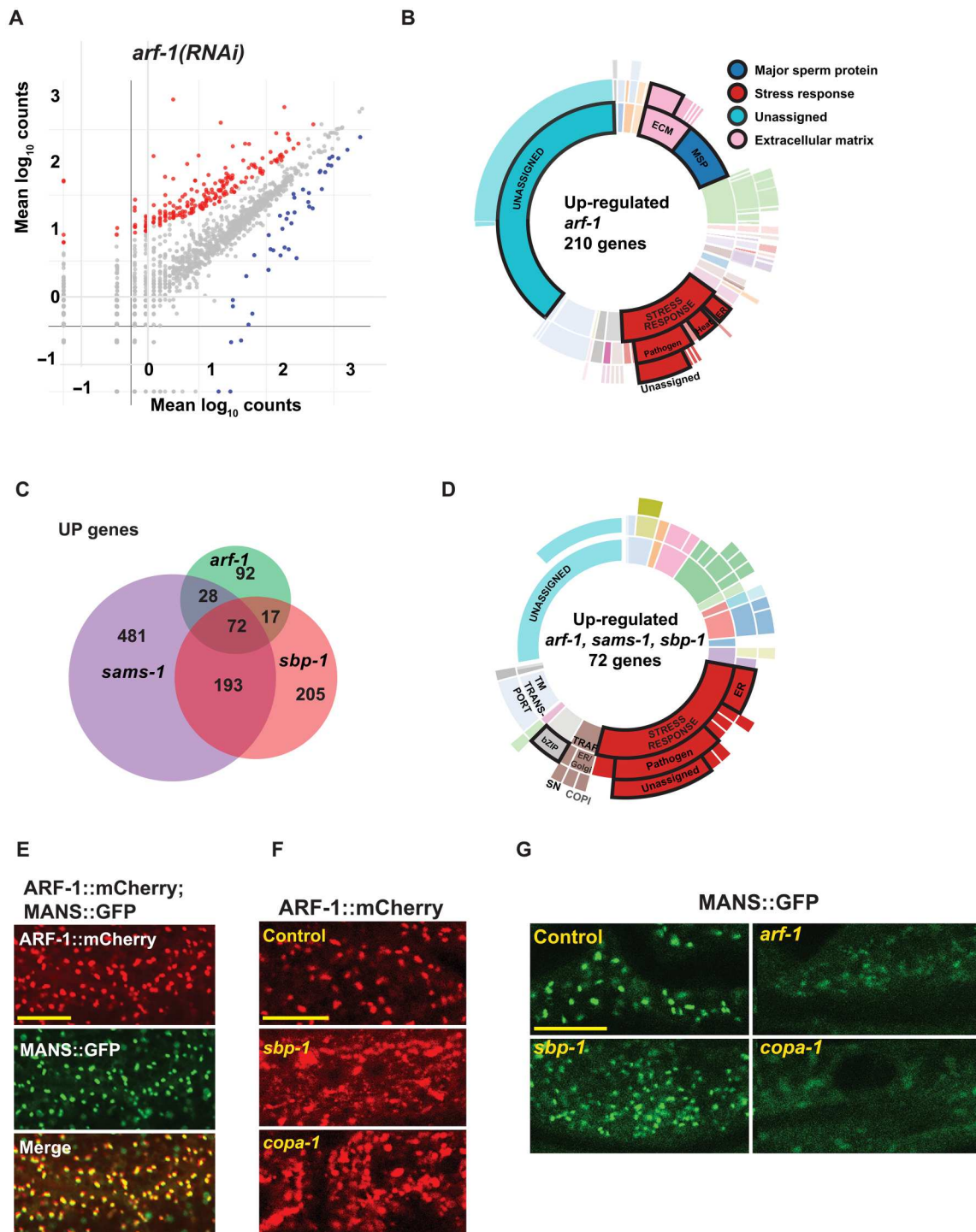


**Fig. 4. Disruption of Golgi function through RNAi of *arf-1* activates ILGs.** (A) Scatter plot shows changes in gene expression after *arf-1* RNAi with genes more than twofold and a false discovery rate less than 0.01 and up-regulated in red with down blue. (B) Sundial diagram of WormCat category enrichment of genes up-regulated after *arf-1* (RNAi). Categories at level 1, 2, or 3 with a significant enrichment (adjusted *P* value < 0.01) are outlined and labeled in the legend. (C) Venn diagram showing overlap of up-regulated genes after *sbp-1*, *sams-1*, or *arf-1* RNAi. (D) Sundial diagram of WormCat category enrichment of up-regulated genes shared between *sams-1*, *sbp-1*, and *arf-1* (RNAi). Categories at level 1, 2, or 3 with a significant enrichment (adjusted *P* value < 0.01) are outlined and labeled in the legend. (E) Confocal projections of endogenously tagged ARF-1::mCherry reveal that that Golgi-like pattern is disrupted after *sbp-1* RNAi and quantitation in fig. S5A. (F) Confocal images of intestinal cells from ARF-1::mCherry; *ges-1*::MANS-1::GFP animals. Scale bar, 10  $\mu$ m for (E) and (F). (G) Confocal projections of the *C. elegans* Golgi marker MANS::GFP (57) in control, *sbp-1*, *arf-1*, and *copa-1* (1:10) RNAi intestines with quantitation of puncta intensity and number in fig. S5 (B and C). Scale bar, 10  $\mu$ m. Significance is determined by the Mann-Whitney test.

(this study) in models of lipid perturbation that lower PC. Thus, blocking or limiting ARF-1 function at the Golgi appears to be a mechanistic step linking changes in levels of membrane lipids, such as PC, and activation of ILGs.

### ILG up-regulation occurs in models of trafficking dysfunction

The Golgi apparatus accepts proteins from the ER destined for secretion, processing them by glycosylation before secretory vesicles are loaded (62). Stimulation of the innate immune system may notably affect trafficking load, as AMPs are shuttled through the membrane trafficking system (63). Activation of the ER stress response has been noted in multiple systems when large numbers of proteins need to be produced and secreted (64). Previous data suggest that induction of membrane stress may also be a sensor of infection (65). On the basis of work by the Ewbank laboratory, Lamitina *et al.* (65, 66) also suggested that some pathogen-response genes act to support the trafficking of AMPs. We noted that the ILGs up-regulated at low PC are largely outside of the antimicrobial categories and comprise gene sets defined by their shared expression upon pathogen exposure rather than function (24, 28). We hypothesize that some of these genes might respond to direct stress on the trafficking system. To explore this idea, we turned to a commonly used system for studying trafficking in *C. elegans*, VIT-2::GFP (67) and comparing ILG gene expression in strains with increasing copy number to simulate an increase in secretory load. *Vit-2* is a vitellogenin produced and secreted from intestinal cells then taken up by the germ line (68). First, we used WormCat to compare category enrichment data from two published studies examining genome-wide mRNA expression patterns when *vit-2* is overexpressed or misregulated, placing stress on the secretory system. The Blackwell laboratory showed that germline-less *glp-1* mutants exhibit *vit-2*::GFP buildup near its production site in the intestines (69). WormCat analysis of their RNA-seq data found strong enrichment patterns in STRESS RESPONSE: Pathogen. (Fig. 5, A and C, and data S4). Next, we used WormCat to examine RNA-seq data from VIT-2::GFP (70)-overexpressing animals produced by the Aballay group and also found increases in the stress response category enrichment (Fig. 5, B and C, and data S4). As two models sharing VIT-2::GFP secretory overload show increases in STRESS RESPONSE: Pathogen genes, we sought to directly test this model by comparing ILG expression in two strains with a differing copy number of *vit-2*, RT130, made by microparticle bombardment and containing the GFP array in addition to wild-type copies (71), and BCN9071, which is a CRISPR-generated allele integrated into the endogenous locus (72) (Fig. 5, D to F). Confocal projections of intestinal cells expressing VIT-2::GFP show a light punctate pattern across the cytoplasm of the intestine showing the yolk particles as they transit the secretory system (Fig. 5D and fig. S5A). VIT-2::GFP appears as intracellular puncta in both single and multicopy strains. However, RNAi of *arf-1*, which disrupts the secretory system, produced larger intracellular aggregates in the multicopy RT130 strain (Fig. 5D), suggesting that this strain is sensitized to stress in the secretory system. Strikingly, the expression of ILGs increases with VIT-2::GFP copy number (Fig. 5, G to J), showing that increasing expression of proteins destined for the secretory pathway is sufficient to induce ILGs.

### Knockdown of STRESS RESPONSE: Pathogen genes disrupt trafficking reporters

We found that ILGs become up-regulated when lipid levels become unbalanced, when ARF-1 functions are compromised, or when the production of secreted proteins increases. This activation mechanism is independent of pathogen exposure. One model could be that alterations in membranes could be part of a surveillance system used by the innate immune system to detect alterations in cellular function indicating a pathogen challenge, as in blocks in translation shown by the Troemel and Ausebel laboratories (73, 74) or addition of ectopic lipids (33). It is also possible that these genes counteract stress on the secretory system, which could occur when the lipids that make up the secretory system are out of balance. As a pilot experiment, we focused on one of the up-regulated genes, *hpo-6*, which is not present in any of the commercially available RNAi libraries. To study its function more closely in this context, we made a cDNA construct to allow RNAi in VIT-2::GFP RT130 in wild-type and *sams-1(lop)* animals (9). *hpo-6* was originally identified in a screen for genes, whose loss increased sensitivity to a pore-forming toxin (75). It has a glycoprotein domain and may occur in membrane rafts (76) but has no apparent homology to human proteins. *Hpo-6(RNAi)* causes a slight increase in VIT-2::GFP puncta in wild-type animals (fig. S5A). However, in the low PC *sams-1(lop)* background, VIT-2::GFP pooling and intracellular aggregation suggest that reduction in *hpo-6* has a broad effect on yolk trafficking out of the intestinal cells.

The puncta increasing in yolk in *C. elegans* consist of both lipids and proteins (77); thus, it is difficult to separate the potential effects. To confirm our results in a less complex model, we turned to the *myo-3*::signal sequence green fluorescent protein(ssGFP) reporter model (78), which expresses and secretes GFP in body wall muscle cells. First, we examined ssGFP in *sbp-1(ep79)*, a hypomorphic allele of *sbp-1* (79). In control animals, ssGFP is secreted and is visible between the striated muscle cells; reduction in *sbp-1* function causes some aggregation of the ssGFP within the cells (Fig. 6, B to D), suggesting that it is not being secreted as efficiently. We noted that this effect was even more pronounced after *arf-1(RNAi)* in both control and *sbp-1(ep79)* backgrounds (Fig. 6, B to D), consistent with the central role of ARF-1 in the secretory process. To test whether the effects of knockdown of ILGs could affect the secretion of this reporter, we conducted a small-scale screen of 19 other STRESS RESPONSE: Pathogen: unassigned genes on secretion in *myo-3*::ssGFP and the sensitized *sbp-1(ep79)*; *myo-3*::GFP backgrounds, imaging body wall muscle cells in triplicate and manually scoring aggregation in blinded samples (Fig. 6A). We selected *hpo-6*, *irg-2*, and ZK6.11/*irg-8* from this initial screen and then validated effects by confocal imaging, blinded visual scoring, and quantitation of puncta size and number with CellProfiler (80). We found that as in *arf-1* RNAi, reduction in *hpo-6*, *irg-2*, and *irg-8/ZK6.11* increased puncta size (Fig. 6, B to D, and fig. S5, D and E), with related decrease in aggregate number in both wild-type and the *sbp-1(ep79)* background, reflecting aggregation and disruption of normal secretory processes. GFP mRNA measured by qRT-PCR did not significantly increase, suggesting posttranscriptional effects (fig. S5F).

Many of the STRESS RESPONSE: Pathogen genes are expressed highly in the intestine; therefore, we also examined a ssGFP expressed under the *glo-1* promoter (81) in adult intestinal cells. Using epifluorescence imaging, we found that intestinal ssGFP

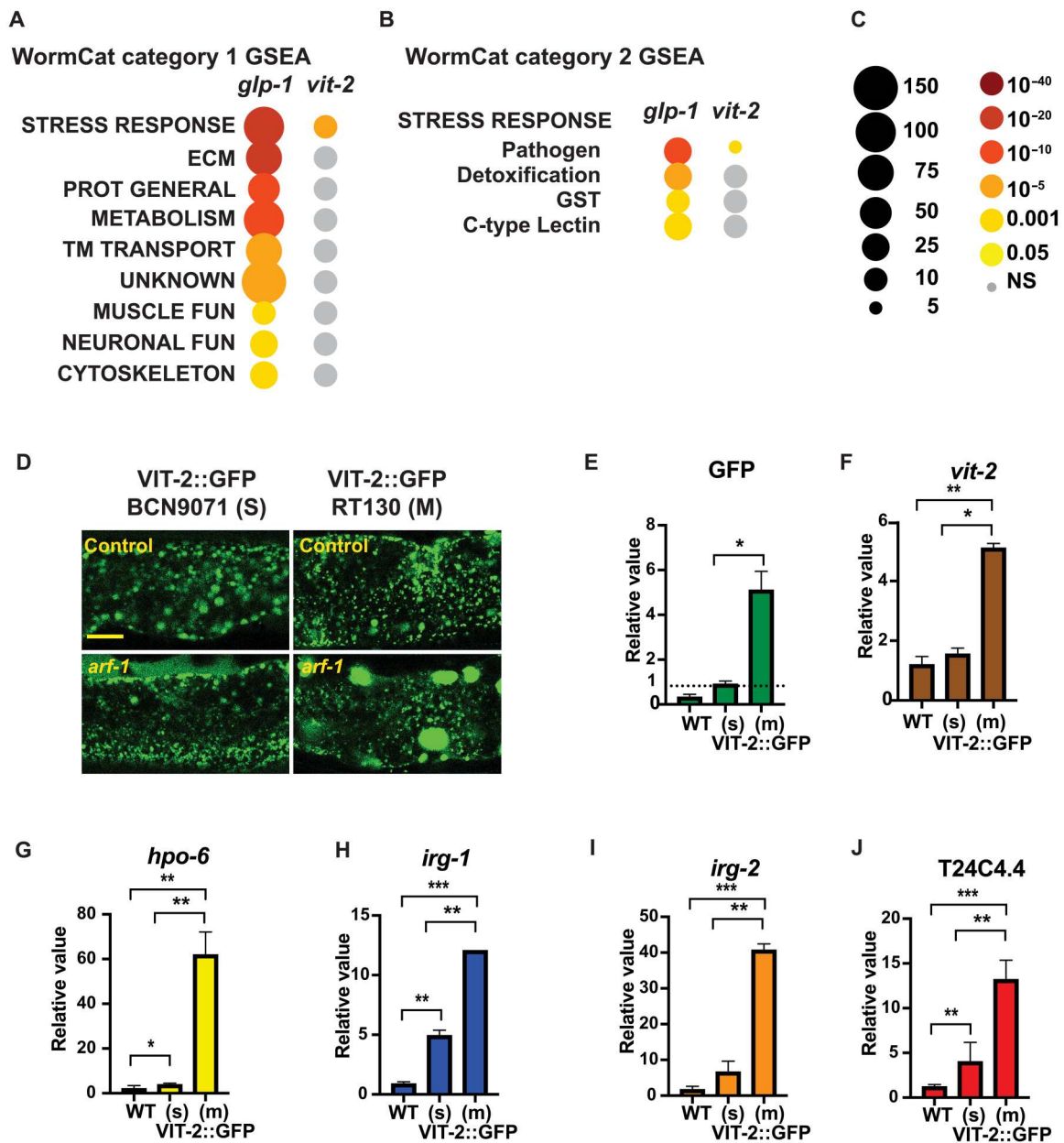


**Fig. 5. ILG expression is linked to trafficking disruption.** WormCat gene enrichment of up-regulated genes from *glp-1*(*e2141ts*) (69) and *vit-2*(*ac3*) compared to SJ4005 (101) for category 1 (A) and category 2 (B). Legend is in (C). (D) Confocal projections of *C. elegans* intestinal cells expressing *vit-2::GFP* (RT130) or *vit-2::GFP* (BCN9071) in wild-type or *arf-1* RNAi animals. qRT-PCR comparing gene expression in wild-type, single copy *vit-2::GFP* (BCN9071, s), or multicopy (RT130, m) animals. Scale bar, 10  $\mu$ m. (E and F) Increase in GFP or *vit-2*. Immune response genes are shown in (F) to (J). Significance is determined by Student's *t* test. GST, glutathione S-transferase. \* $P < 0.05$  and \*\* $P < 0.01$ .

accumulated after RNAi of *sbp-1*, *arf-1*, *hpo-6*, *irg-2*, and *irg-8* (Fig. 6, E and F). Although ssGFP mRNA increased in *hpo-6* animals, there were minimal changes after *arf-1* RNAi, showing that mRNA levels did not correlate with GFP fluorescence (fig. S5C). Last, we used confocal imaging to examine ssGFP at a greater resolution for one of these genes, *hpo-6*, along with *sbp-1*. We found that control animals showed small puncta of the ssGFP in the cytoplasm of the intestinal cells, which accumulated and became larger when the lipids metabolism was disrupted by *sbp-1* or after *hpo-6* RNAi (Fig. 6, G and H). High-level expression of GFP

that is not targeted to the secretory pathway does not normally aggregate, suggesting that this is not simply a result of overexpression (see Fig. 3A). Thus, in a variety of cell types, we find that interference with *sbp-1*, or candidate STRESS RESPONSE: Pathogen genes, causes aggregation and pooling of ssGFP in the absence of pathogen stimulation, suggesting a role in secretory processes.

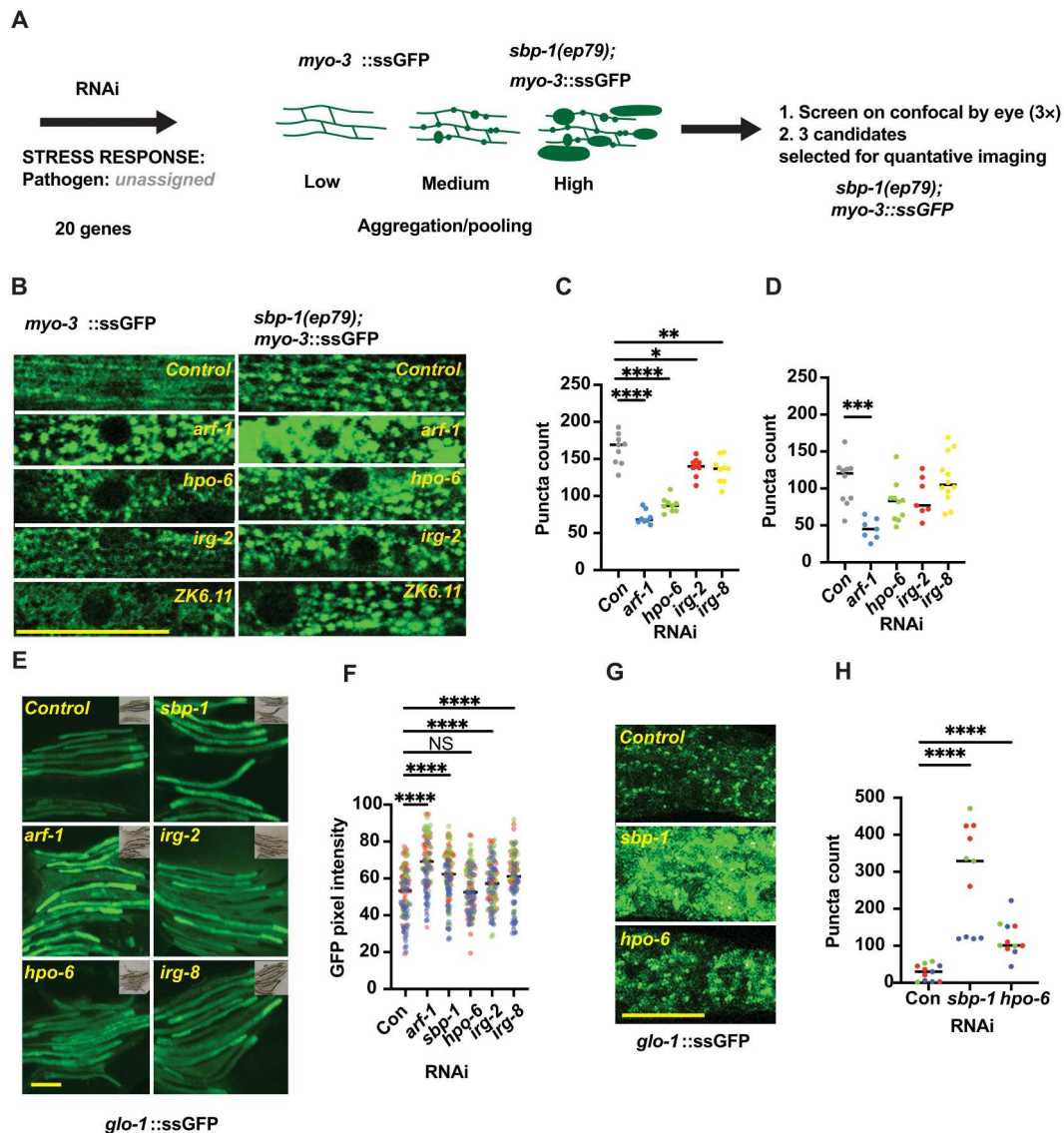


**Fig. 6. RNAi of selected ILGs enhances aggregation of secreted reporters.** (A) Schematic diagram of small-scale screen of STRESS RESPONSE: Pathogen: *unassigned* genes for aggregation of a secreted reporter in body wall muscle (*myo-3::ssGFP*). Confocal projections of ssGFP in body wall muscle in control or the *sbp-1(ep79)* background (B). Quantification of three independent replicates by CellProfiler determining number of puncta (C and D) and puncta area (fig. S5, D and E). Scale bar, 10  $\mu$ m for (B), (E), and (G). (E) Epifluorescence images of ssGFP expressed from an intestinal reporter with DIC images as insets. Quantitation of pixel intensity with ImageJ is in (F). Confocal projections showing ssGFP aggregation in (G), with puncta quantitation by CellProfiler in (H). Significance is determined by the Mann-Whitney test. \* $P < 0.05$  and \*\* $P < 0.01$ .

### Knockdown of STRESS RESPONSE: Pathogen genes affect an endogenous PA14-stimulated peptide

The secretory pathway carries out many basal functions and must increase capacity during stresses requiring protein production increases, such as pathogen challenge. The ER stress pathway plays a key role during this increase (82, 83), and our results suggest that alterations in the Golgi may also be sensed and result in the up-regulation of ILGs. Our studies of ssGFP reporters allowed the isolation of the effects of lipid imbalances on basal secretory processes from the complex response to pathogens. However, ILGs are defined by high-level expression upon pathogen exposure and could also affect the secretion of AMPs or other defensive

molecules. *C. elegans* contains a large number of proteins with domains common to AMPs, such as ShKT, Sushi, and CUB domains (84). To test the effects of the ILGs on an endogenous secreted protein in the pathogen response, we selected C32H11.9/*clد-1* (cub-like domain 1). In our previous RNA-seq experiments, it was the highest up-regulated gene after PA14 exposures (Fig. 7A). It was also strongly induced during other early time points (23) but not induced by lipid imbalances in *sbp-1(RNAi)* animals (Fig. 7B). It contains a signal sequence, suggesting that CLD-1 is secreted, as well as a CUB domain, common to antimicrobial proteins (Fig. 7C). We obtained an allele with GFP fused to the C terminus of *clد-1/C32H11.6* using CRISPR [PHX2081(C32H11.6::GFP

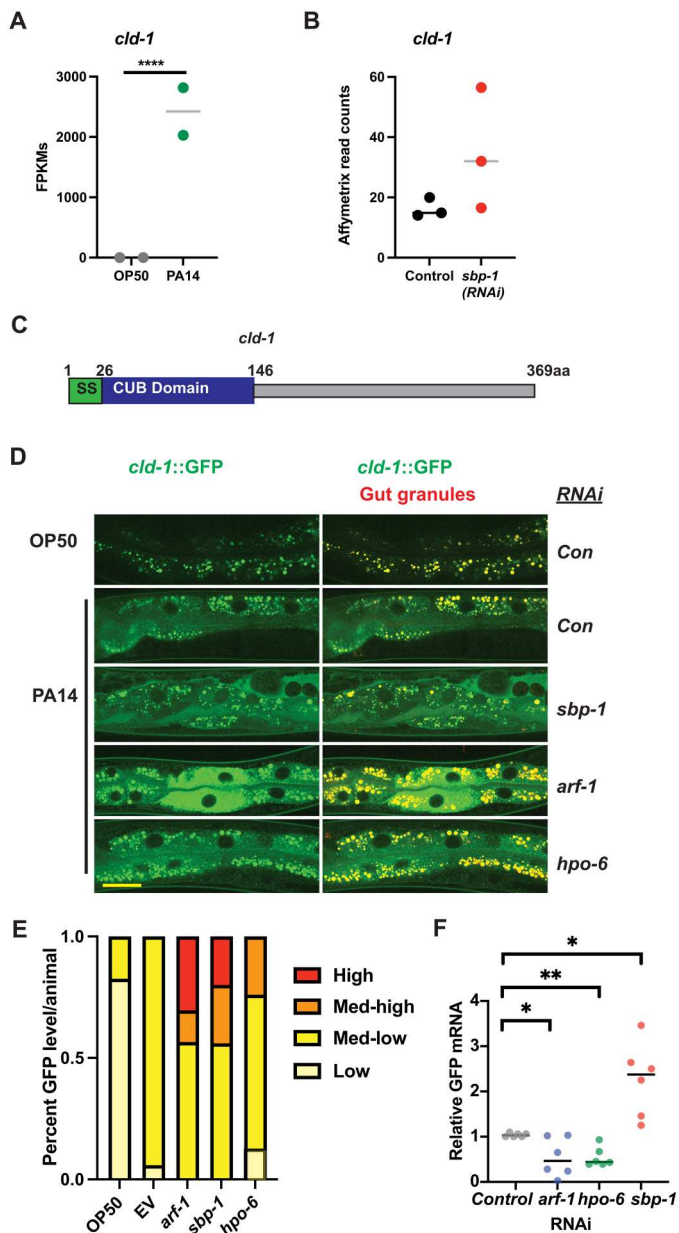


**Fig. 7. Interference with secretory function or knockdown of selected ILGs can enhance intestinal accumulation of a *Pseudomonas*-induced CUB domain protein.** Expression of *cld-1*/C32H9.11 in response to *Pseudomonas aeruginosa* (PA14) from Ding et al. (9) (A) or after *sbp-1* RNAi from Ding et al. (9) (B). (C) Domain structure of CLD-1 showing signal sequence and CUB domain. (D) Spinning disc confocal micrographs showing intestinal accumulation of *cld-1::GFP* in response to PA14 after *sbp-1*, *arf-1*, or ILG RNAi taken at 488 nm. Gut granules are shown with an overlay of a micrograph of the same section from taken at 564 nm. Scale bar, 10  $\mu$ m. Blinded scoring of animals for increased fluorescence and aggregation is in (E). (F) qPCR showing levels of GFP mRNA expression. Error bars show SD, statistical relevance of individual RNAi to control calculated by paired t test in GraphPad Prism.

(*sybIS7080*), which accumulated in the intestine after PA14 exposure (Fig. 7D), consistent with disruption with secretion. Notably, RNAi of *sbp-1* disrupted CLD-1::GFP production, causing increases in total levels, intracellular aggregation, and accumulation in the pseudocoelom, consistent with defects in secretory processes (Fig. 7D). Knockdown of *arf-1* also produced similar effects, strengthening these links. Interference with *hpo-6*, a candidate ILG, also caused accumulation and aggregation of CLD-1::GFP during PA14 exposure. Notably, mRNA expression patterns showed that expression of the GFP transcript did not vary with the same pattern as the GFP fluorescence, showing that increases in gene expression could not explain changes in GFP protein. Together, this suggests that some ILG genes act to support secretory function during stress, which may be initiated by lipid imbalances or by pathogen exposure.

## DISCUSSION

Membrane lipids form the organelles of the secretory system, which can sense changes in protein homeostasis or lipids levels and elicit gene expression programs when stressed. Multiple well-studied pathways are linked to changes in proteostasis or lipid levels within the ER (64). These processes are orchestrated by ER-intrinsic proteins that sense changes in protein folding or alterations in the lipid bilayer (6, 7, 16, 85). These ER-linked events are also important during pathogen exposure in *C. elegans*; changes in ribosomal function at the ER have a well-defined impact on pathogen responses (73, 74) and pathogen responses depend on ER stress pathways to protect this organelle from the demands of the immune response (83, 86). The Lee laboratory also found that ILGs are up-regulated when trafficking is inhibited by blocking ER glycosylation (87). In addition, pathogen responses require an intact ER stress pathway to allow adjustment to the increased trafficking load (65, 83), as AMPs are produced in mass in the ER, sent in lipid vesicles to the Golgi, where many are glycosylated and then packaged into lipid vesicles for secretion (88). For example, the *C. elegans* genome contains more than 300 genes produced in response to specific pathogens that share similarities to known antimicrobial effectors (89). However, many of the genes in the *C. elegans* innate immune response do not have obvious similarity to antimicrobial effectors and are defined solely as being responsive pathogens (28, 90). It is this class that is largely shared between pathogen-induced and membrane stress-induced stress programs. Several lines of evidence prompted us to hypothesize that some of these genes might be part of a response linked to stress in membranes of the secretory pathway rather than a direct response to an extrinsic pathogen. First, the involvement of secretory organs was implicated by alterations in PC ratios in the ER/Golgi in both *sams-1* and *sbp-1* RNAi lipidomes. Second, our targeted RNAi screen for regulators of *psysm-1::GFP* identified the *arf-1* GTPase and coatamer proteins, which are critical for Golgi/ER transport. The knockdown of *arf-1* was sufficient to induce ILG up-regulation. Strengthening this link between disruption of lipid levels and ARF-1 function, we also found that *sbp-1* RNAi altered ARF-1::mCherry localization and Golgi morphology.

Other organelles in the secretory pathway, such as the Golgi, have their own stress sensors and response pathways (91), some of which act by affecting the ARF1 GTPase (92). ARF-1 is a critical regulator of trafficking, coordinating retrograde traffic from the Golgi to the ER and regulating secretory function in the trans-

Golgi (93). Cycling of ARF-1 GTPases depends on membrane localization of the ARF GTPase, guanine exchange factor (GEF), and GTPase activating protein (GAP) (93). We previously found that the knockdown of PC synthesis enzymes blocked ARF1 cycling and limited membrane association of the ARF GEF GBF1 in cultured human cells (10). This suggests that low PC levels affect ARF1 activity by limiting the ability of the GTPase, GEF, and GAP to associate at the Golgi membrane and initiate guanosine diphosphate–guanosine 5'-triphosphate cycling. However, PC could be linked to ARF1 through other mechanisms. ARF1 and phospholipase D (PLD) function have been linked by multiple laboratories (94). PLD cleaves PC molecules to produce choline and phosphatidic acid, which in turn stimulates vesicle formation (95). This regulatory loop requires PC, which is low in ER/Golgi membranes in *sams-1* and *sbp-1* RNAi animals. DAG kinases, which could be stimulated by changes in DAGs in the *sbp-1* or *sams-1*(RNAi) animals, can also affect ARF activity and trafficking (96). Last, protein kinase D (PKD) has an important role in maintaining Golgi structure, and its ortholog has been linked to immunity in *C. elegans* (97, 98). However, loss of DAG kinases or PKD failed to activate the *psysm-1::GFP* reporter in our RNAi screen, suggesting that they could be important in other regulatory contexts. While the lipidomic changes in *sbp-1* and *sams-1* animals are broad and individual lipids could act through multiple independent mechanisms, our results show that decreasing PC is sufficient to limit ARF-1 function (10) and activate ILG expression in the absence of pathogen.

Pathogen-elicited gene expression programs are part of a specialized stress response where specific sets of AMPs are produced and then secreted in response to pathogens. This type of innate immune response initiates as pathogens are recognized by interaction with cellular proteins or cellular processes are disturbed (99). In *C. elegans*, evidence for microbe/pathogen-associated molecular patterns has been less clear. Instead, *C. elegans* rely on surveillance of cellular processes such as translation that are affected by pathogenic attack (73). Lipid imbalances caused by exogenous cholesterol have been suggested to act as a similar intracellular signal in recent studies (33). However, alterations in PC leading to activation of pathogen-responsive genes do not necessarily confer pathogen resistance (9), and ILG expression levels are much lower than what occurs in a pathogen response. Many of the ILGs, for example, those in the STRESS RESPONSE: Pathogen: unassigned WormCat categories (27, 28), lack domains associated with AMP function. While some could have antimicrobial properties with distinct motifs, the activation of these genes through intrinsic stress in the Golgi prompted us to ask if others acted to support secretory function. Our data showing that reduction of *hpo-6*, *irg-2*, and *irg-8* increased aggregation and pooling of secreted reporters and endogenous proteins secreted in an immune response in control suggest that they could protect or support secretory function occurring after broad disruption in membrane lipids or after pathogen exposure occurs. Thus, some ILGs may function in a "multimembrane" stress response encompassing the roles of both the ER and the Golgi in trafficking. Together, these results illustrate mechanisms linking lipid metabolism to genes activated in the immune response through effects on the secretory system.

## MATERIALS AND METHODS

### *C. elegans* strains, RNAi constructs, and screening

N2 (wild type), *psysm-1::GFP* (AU78), *myo-3::GFP* (GS1912), MANS::GFP (RT1315), and OP50-1 were obtained from the *Caenorhabditis* Genetics Center. Exglo-1::ssGFP (GH639) was a gift from G. Hermann (Lewis and Clark University). *myo-3::ssGFP;sbp-1* (*ep79*) (WAL510) was constructed in this study. CRISPR-tagged ARF-1, *parf-1::ARF-1::mCherry* (*knu418*), was obtained from the In Vivo Biosystems (COP1415) and then outcrossed three times (WAL10). Imaging of MANS::GFP was done from a strain also harboring a CRISPR-tagged *warf-1::RFP* (*ker4*) (WAL12). WAL511 was constructed by crossing MANS::GFP and WAL510 (*parf-1::ARF-1::mCherry* (*knu418*)). *clt-1/C32H11.6::GFP* was constructed by SUNY Biotech using CRISPR [PHX2081(*sybIS7080*)]. Normal growth media (NGM) was used unless otherwise noted. For RNAi, gravid adults were bleached onto NGM plates supplemented with ampicillin, tetracycline, 6 mM isopropyl-β-D-thiogalactopyranoside, and 10× concentrated bacterial cultures. *C. elegans* were allowed to develop until the young adult stage before harvesting. Because of larval arrest, *copa-1* RNAi bacteria were diluted 1:10 in control RNAi bacteria before plating. For the RNAi screen of *psysm-1::GFP*, L1 larvae were plated into 96-well plates spotted with RNAi bacteria, and L4/young adults were scored from −3 to +3 with 0 as no change in four independent replicates on a Zeiss GFP dissecting scope with an Axiocam camera. Candidates that were positive in three-fourth replicates were tested an additional four times, imaging three sets of 10 animals per RNAi. Image quantitation is described below. For the RNAi screen of *myo-3::ssGFP* and *myo-3::ssGFP; sbp-1*(*ep79*), four independent replicates were subjected to RNAi, placed in channeled agarose pads, and confocal images were collected on a Leica SP6.

### Cell culture and siRNA transfection

HepG2 cells (American Type Culture Collection, HB-8065) were grown in minimum essential medium (Invitrogen) plus 10% fetal bovine serum (Invitrogen), glutamine (Invitrogen), and sodium pyruvate (Invitrogen). siRNA oligonucleotides transfections were done for 48 hours using Lipofectamine RNAiMAX Transfection Reagent (Invitrogen, 13778100), and cells were held for 16 hours in 1% lipoprotein-deficient serum (Biomedical Technologies, BT907) and ALLN (25 μg/ml; Calbiochem) for 30 min before harvesting.

### Immunoblotting

#### HepG2 cells

Syringe passage was used to lyse cells in high-salt radioimmunoprecipitation assay (RIPA) [50 mM Tris (pH 7.4), 400 mM NaCl, 0.1% SDS, 0.5% Na-deoxycholate, 1% NP-40, 1 mM DTT, ALLN (2.5 μg/ml), and complete protease inhibitors (Roche)]. Invitrogen NuPage gels (4 to 12%) were used for protein separation before transfer to nitrocellulose. Blots were probed with antibodies to phosphorylated p38 MAP Kinase, and total p38 and signal transducers and activators of transcription 1 were used as a control. Immune complexes were visualized with Luminol Reagent (Millipore). Densitometry was performed by scanning the film and then pixel intensity analysis with ImageJ software. Graphs show the average of at least three independent experiments with control values normalized to one.

### Whole *C. elegans*

Young adult animals were lysed by sonication in high-salt RIPA, and immunoblotting was performed as above.

### Microscopy and image quantitation

ARF-1::mCherry, MANS-1::GFP, and ssGFP images were acquired on a Leica SPE confocal, and projections of confocal slices were produced. All images were taken at identical gain settings within experimental sets, and Adobe Photoshop was used to correct levels across experimental sets. Image quantitation of GFP fluorescence was done using Fiji/ImageJ2. Briefly, each photo was processed individually, beginning by splitting the image into three color channels (red/green/blue) and choosing the green channel for analysis. This image was then converted to an eight-bit gray image and processed using the function "Enhance Local Contrast (CLAHE)" [block size: 250, histogram bins: 256, max slope: 5.00, mask: none, fast (less accurate): no (unchecked)]. Using the circle selection tool, four sections (width: 55; height: 25) of the brightest areas across each worm's intestine were selected from this processed image and measured for intensity (integrated intensity). One additional section was taken from beside each worm to account for background fluorescence. The background reading was subtracted from each individual intestinal reading, then the four corrected readings were added to get a sum of fluorescent intensity. Imaging of C32H11.9/*clt-1*::GFP was performed on a W1 Yokogawa spinning disk confocal microscope equipped with a Photometrics Prime BSI Express scientific complementary metal-oxide semiconductor camera. Quantitation was performed with Nikon Imaging System software. Statistical tests performed include normality and log normality tests (Anderson-Darling, D'Agostino & Pearson, Shapiro-Wilk, and Kolmogorov-Smirnov) and Mann-Whitney tests.

### Lipidomics

*C. elegans* total and microsomal lipidomics, including fractionation protocols, were performed at the Whitehead Metabolomics core as in (10). Enrichment of ER or Golgi proteins was confirmed by immunoblotting with antibodies to SQV-8/B3GAT3 and CNX-1/Calnexin obtained from the Developmental Studies Hybridoma Bank. Statistical analysis was performed in GraphPad Prism.

### Gene expression analysis

Lysis of young adult *C. elegans* was performed in 0.5% SDS, 5% beta mercapto ethanol ( $\beta$ -ME), 10 mM EDTA, 10 mM tris-HCl (pH 7.4), and proteinase K (0.5 mg/ml) before purification of RNA by TRI-Reagent (Sigma-Aldrich). cDNA was produced with Transcriptor First-strand cDNA kits (Roche), and RT-PCR was performed using Kappa SYBR Green 2X Mastermix. qRT-PCR was performed on an Eppendorf RealPlex<sup>2</sup>.

RNA for sequencing was purified using RNeasy columns (QIAGEN). RNA-seq, including library construction, was performed by BGI (Hong Kong). Reads were analyzed through the Dolphin analysis platform using DeSeq to identify differentially expressed genes (100). Gene set enrichment was performed using WormCat (www.wormcat.com) (27, 28). The Gene Expression Omnibus (GEO) accession number is GSE242371.

### Supplementary Materials

This PDF file includes:

Figs. S1 to S5

Legends for data S1 to S4

Other Supplementary Material for this manuscript includes the following:

Data S1 to S4

### REFERENCES AND NOTES

1. K. E. Wellen, C. B. Thompson, Cellular metabolic stress: Considering how cells respond to nutrient Excess. *Mol. Cell* **40**, 323–332 (2010).
2. J. Aramburu, M. C. Ortells, S. Tejedor, M. Buxadé, C. López-Rodríguez, Transcriptional regulation of the stress response by mTOR. *Sci. Signal.* **7**, re2 (2014).
3. H. G. Son, O. Altintas, E. J. E. Kim, S. Kwon, S. J. V. Lee, Age-dependent changes and biomarkers of aging in *Caenorhabditis elegans*. *Aging Cell* **18**, e12853 (2019).
4. K. Halbleib, K. Pesek, R. Covino, H. F. Hofbauer, D. Wunnicke, I. Hänel, G. Hummer, R. Ernst, Activation of the unfolded protein response by lipid bilayer stress. *Mol. Cell* **67**, 673–684. e8 (2017).
5. M. A. Gianfrancesco, N. Paquot, J. Piette, S. Legrand-Poels, Lipid bilayer stress in obesity-linked inflammatory and metabolic disorders. *Biochem. Pharmacol.* **153**, 168–183 (2018).
6. J. H. Koh, L. Wang, C. Beaudoin-Chabot, G. Thibault, Lipid bilayer stress-activated IRE-1 modulates autophagy during endoplasmic reticulum stress. *J. Cell Sci.* **131**, jcs217992 (2018).
7. G. S. Hotamisligil, R. J. Davis, Cell signaling and stress responses. *Cold Spring Harb. Perspect. Biol.* **8**, a006072 (2016).
8. T. Radanović, J. Reinhard, S. Ballweg, K. Pesek, R. Ernst, An emerging group of membrane property sensors controls the physical state of organellar membranes to maintain their identity. *Bioessays* **40**, e1700250 (2018).
9. W. Ding, L. J. Smulan, N. S. Hou, S. Taubert, J. L. Watts, A. K. Walker, S-Adenosylmethionine levels govern innate immunity through distinct methylation-dependent pathways. *Cell Metab.* **22**, 633–645 (2015).
10. L. J. Smulan, W. Ding, E. Freinkman, S. Gujja, Y. J. K. Edwards, A. K. Walker, Cholesterol-independent SREBP-1 maturation is linked to ARF1 inactivation. *Cell Rep.* **16**, 9–18 (2016).
11. A. K. Walker, R. L. Jacobs, J. L. Watts, V. Rottiers, K. Jiang, D. M. Finnegan, T. Shioda, M. Hansen, F. Yang, L. J. Niebergall, D. E. Vance, M. Tzoneva, A. C. Hart, A. M. Näär, A conserved SREBP-1/phosphatidylcholine feedback circuit regulates lipogenesis in metazoans. *Cell* **147**, 840–852 (2011).
12. J. D. Horton, J. L. Goldstein, M. S. Brown, SREBPs: Activators of the complete program of cholesterol and fatty acid synthesis in the liver. *J. Clin. Investig.* **109**, 1125–1131 (2002).
13. F. Yang, B. W. Vought, J. S. Satterlee, A. K. Walker, Z. Y. J. Sun, J. L. Watts, R. DeBeaumont, R. M. Saito, S. G. Hyberts, S. Yang, C. Macol, L. Iyer, R. Tjian, S. van den Heuvel, A. C. Hart, G. Wagner, A. M. Näär, An ARC/Mediator subunit required for SREBP control of cholesterol and lipid homeostasis. *Nature* **442**, 700–704 (2006).
14. R. M. McKay, J. P. McKay, L. Avery, J. M. Graff, C. *elegans*: A model for exploring the genetics of fat storage. *Dev. Cell* **4**, 131–142 (2003).
15. S. Wu, A. M. Näär, SREBP1-dependent de novo fatty acid synthesis gene expression is elevated in malignant melanoma and represents a cellular survival trait. *Sci. Rep.* **9**, 10369 (2019).
16. N. Ho, W. S. Yap, J. Xu, H. Wu, J. H. Koh, W. W. B. Goh, B. George, S. C. Chong, S. Taubert, G. Thibault, Stress sensor Ire1 deploys a divergent transcriptional program in response to lipid bilayer stress. *J. Cell Biol.* **219**, e201909165 (2020).
17. Y. Jung, S. Kwon, S. Ham, D. Lee, H. E. H. Park, Y. Yamaoka, D. E. Jeong, M. Artan, O. Altintas, S. Park, W. Hwang, Y. Lee, H. G. Son, S. W. A. An, E. J. E. Kim, M. Seo, S. J. V. Lee, *Caenorhabditis elegans* Lipin 1 moderates the lifespan-shortening effects of dietary glucose by maintaining  $\omega$ -6 polyunsaturated fatty acids. *Aging Cell* **19**, e13150 (2020).
18. J. D. Nhan, C. D. Turner, S. M. Anderson, C.-A. Yen, H. M. Dalton, H. K. Cheesman, D. L. Ruter, N. U. Naresch, C. M. Haynes, A. A. Soukas, R. Pukkila-Worley, S. P. Curran, Redirection of SKN-1 abates the negative metabolic outcomes of a perceived pathogen infection. *Proc. Natl. Acad. Sci. U.S.A.* **116**, 22322–22330 (2019).
19. Z. Wu, M. Isik, N. Moroz, M. J. Steinbaugh, P. Zhang, T. K. Blackwell, Dietary restriction extends lifespan through metabolic regulation of innate immunity. *Cell Metab.* **29**, 1192–1205.e8 (2019).
20. I. Engelmann, A. Griffon, L. Tichit, F. Montañana-Sanchis, G. Wang, V. Reinke, R. H. Waterston, L. W. Hillier, J. J. Ewbank, A comprehensive analysis of gene expression changes provoked by bacterial and fungal infection in *C. elegans*. *PLOS ONE* **6**, e19055 (2011).

21. G. V. Mallo, C. L. Kurz, C. Couillaud, N. Pujol, S. Granjeaud, Y. Kohara, J. J. Ewbank, Inducible antibacterial defense system in *C. elegans*. *Curr. Biol.* **12**, 1209–1214 (2002).
22. M. Fletcher, E. J. Tillman, V. L. Butty, S. S. Levine, D. H. Kim, Global transcriptional regulation of innate immunity by ATF-7 in *C. elegans*. *PLoS Genet.* **15**, e1007830 (2019).
23. E. R. Troemel, S. W. Chu, V. Reinke, S. S. Lee, F. M. Ausubel, D. H. Kim, p38 MAPK regulates expression of immune response genes and contributes to longevity in *C. elegans*. *PLoS Genet.* **2**, e183 (2006).
24. K. A. Estes, T. L. Dunbar, J. R. Powell, F. M. Ausubel, E. R. Troemel, bZIP transcription factor zip-2 mediates an early response to *Pseudomonas aeruginosa* infection in *Caenorhabditis elegans*. *Proc. Natl. Acad. Sci. U.S.A.* **107**, 2153–2158 (2010).
25. R. P. Shivers, T. Kooistra, S. W. Chu, D. J. Pagano, D. H. Kim, Tissue-specific activities of an immune signaling module regulate physiological responses to pathogenic and nutritional bacteria in *C. elegans*. *Cell Host Microbe* **6**, 321–330 (2009).
26. N. Zmora, S. Bashirdes, M. Levy, E. Elinav, The role of the immune system in metabolic health and disease. *Cell Metab.* **25**, 506–521 (2017).
27. D. P. Higgins, C. M. Weisman, D. S. Lui, F. A. D'Agostino, A. K. Walker, Defining characteristics and conservation of poorly annotated genes in *Caenorhabditis elegans* using WormCat 2.0. *Genetics* **221**, iyac085 (2022).
28. A. D. Holdorf, D. P. Higgins, A. C. Hart, P. R. Boag, G. J. Pazour, A. J. M. Walhout, A. K. Walker, WormCat: An online tool for annotation and visualization of *Caenorhabditis elegans* genome-scale data. *Genetics* **214**, 279–294 (2019).
29. S. Taubert, M. R. V. Gilst, M. Hansen, K. R. Yamamoto, A Mediator subunit, MDT-15, integrates regulation of fatty acid metabolism by NHR-49-dependent and -independent pathways in *C. elegans*. *Genes Dev.* **20**, 1137–1149 (2006).
30. G. Y. S. Goh, J. J. Winter, F. Bhanshali, K. R. S. Doering, R. Lai, K. Lee, E. A. Veal, S. Taubert, NHR-49/HNF4 integrates regulation of fatty acid metabolism with a protective transcriptional response to oxidative stress and fasting. *Aging Cell* **17**, e12743 (2018).
31. M. L. Ladage, S. D. King, D. J. Burks, D. L. Quan, A. M. Garcia, R. K. Azad, P. A. Padilla, Glucose or altered ceramide biosynthesis mediate oxygen deprivation sensitivity through novel pathways revealed by transcriptome analysis in *Caenorhabditis elegans*. *G3* **6**, 3149–3160 (2016).
32. Y. J. Liu, A. W. Gao, R. L. Smith, G. E. Janssens, D. M. Panneman, A. Jongejan, M. van Weeghel, F. M. Vaz, M. J. Silvestrini, L. R. Lapierre, A. W. MacInnes, R. H. Houtkooper, Reduced ech-6 expression attenuates fat-induced lifespan shortening in *C. elegans*. *Sci. Rep.* **12**, 3350 (2022).
33. N. D. Peterson, J. D. Ico, J. E. Salisbury, T. Rodríguez, P. R. Thompson, R. Pukkila-Worley, Pathogen infection and cholesterol deficiency activate the *C. elegans* p38 immune pathway through a TIR-1/SARM1 phase transition. *eLife* **11**, e74206 (2022).
34. X. Shen, R. E. Ellis, K. Sakaki, R. J. Kaufman, Genetic interactions due to constitutive and inducible gene regulation mediated by the unfolded protein response in *C. elegans*. *PLoS Genet.* **1**, e37 (2005).
35. J. D. Horton, J. L. Goldstein, M. S. Brown, SREBPs: Transcriptional mediators of lipid homeostasis. *Cold Spring Harb. Symp. Quant. Biol.* **67**, 491–498 (2002).
36. H. M. Crook-McMahon, M. Oláhová, E. L. Button, J. J. Winter, E. A. Veal, Genome-wide screening identifies new genes required for stress-induced phase 2 detoxification gene expression in animals. *BMC Biol.* **12**, 64 (2014).
37. Q. Hu, D. R. D'Amora, L. T. MacNeil, A. J. M. Walhout, T. J. Kubiseski, The oxidative stress response in *Caenorhabditis elegans* requires the GATA transcription factor ELT-3 and SKN-1/Nrf2. *Genetics* **206**, 1909–1922 (2017).
38. E. C. Park, C. Rongo, The p38 MAP kinase pathway modulates the hypoxia response and glutamate receptor trafficking in aging neurons. *eLife* **5**, e12010 (2016).
39. A. Mertenskötter, A. Keshet, P. Gerke, R. J. Paul, The p38 MAPK PMK-1 shows heat-induced nuclear translocation, supports chaperone expression, and affects the heat tolerance of *Caenorhabditis elegans*. *Cell Stress Chaperones* **18**, 293–306 (2013).
40. J. C. M. Holthuis, A. K. Menon, Lipid landscapes and pipelines in membrane homeostasis. *Nature* **510**, 48–57 (2014).
41. D. Casares, P. V. Escribá, C. A. Rosselló, Membrane lipid composition: Effect on membrane and organelle structure, function and compartmentalization and therapeutic avenues. *Int. J. Mol. Sci.* **20**, 2167 (2019).
42. G. Hadwiger, S. Dour, S. Arur, P. Fox, M. L. Nonet, A monoclonal antibody toolkit for *C. elegans*. *PLoS ONE* **5**, e10161 (2010).
43. D. E. Jeong, D. Lee, S. Y. Hwang, Y. Lee, J. E. Lee, M. Seo, W. Hwang, K. Seo, A. B. Hwang, M. Artan, H. G. Son, J. H. Jo, H. Baek, Y. M. Oh, Y. Ryu, H. J. Kim, C. M. Ha, J. Y. Yoo, S. J. V. Lee, Mitochondrial chaperone HSP-60 regulates anti-bacterial immunity via p38 MAP kinase signaling. *EMBO J.* **36**, 1046–1065 (2017).
44. C. L. Pender, H. R. Horvitz, Hypoxia-inducible factor cell non-autonomously regulates *C. elegans* stress responses and behavior via a nuclear receptor. *eLife* **7**, e36828 (2018).
45. J. L. Watts, J. Browse, Genetic dissection of polyunsaturated fatty acid synthesis in *Caenorhabditis elegans*. *Proc. Natl. Acad. Sci. U.S.A.* **99**, 5854–5859 (2002).
46. M. Ruiz, R. Bodhicharla, E. Svensk, R. Devkota, K. Busayavalasa, H. Palmgren, M. Ståhlman, J. Boren, M. Pilon, Membrane fluidity is regulated by the *C. elegans* transmembrane protein FLD-1 and its human homologs TLCD1/2. *eLife* **7**, e40686 (2018).
47. R. Bodhicharla, R. Devkota, M. Ruiz, M. Pilon, Membrane fluidity is regulated cell non autonomously by *Caenorhabditis elegans* PAQR-2 and its mammalian homolog AdipoR2. *Genetics* **210**, 189–201 (2018).
48. N. Ho, C. Xu, G. Thibault, From the unfolded protein response to metabolic diseases – Lipids under the spotlight. *J. Cell Sci.* **131**, jcs199307 (2018).
49. R. G. Cutler, K. W. Thompson, S. Camandola, K. T. Mack, M. P. Mattson, Sphingolipid metabolism regulates development and lifespan in *Caenorhabditis elegans*. *Mech. Ageing Dev.* **143–144**, 9–18 (2014).
50. J. Radeny, J. Chan, The role of sphingolipid metabolism in lifespan and healthspan extension in *C. elegans*. *FASEB J.* **33**, 794.16–794.16 (2019).
51. Y. Liu, B. S. Samuel, P. C. Breen, G. Ruvkun, *Caenorhabditis elegans* pathways that surveil and defend mitochondria. *Nature* **508**, 406–410 (2014).
52. A. Spang, ARF1 regulatory factors and COPI vesicle formation. *Curr. Opin. Cell Biol.* **14**, 423–427 (2002).
53. A. G. Fraser, R. S. Kamath, P. Zipperlen, M. Martinez-Campos, M. Sohrmann, J. Ahinger, Functional genomic analysis of *C. elegans* chromosome I by systematic RNA interference. *Nature* **408**, 325–330 (2000).
54. M. A. Gustafson, J. C. Fromme, Regulation of Arf activation occurs via distinct mechanisms at early and late Golgi compartments. *Mol. Biol. Cell* **28**, 3660–3671 (2017).
55. M. M. Rolls, D. H. Hall, M. Victor, E. H. K. Stelzer, T. A. Rapoport, Targeting of rough endoplasmic reticulum membrane proteins and ribosomes in invertebrate neurons. *Mol. Biol. Cell* **13**, 1778–1791 (2002).
56. J. R. Broekhuis, S. Rademakers, J. Burghoorn, G. Jansen, SQL-1, homologue of the Golgi protein GMAP210, modulates intraflagellar transport in *C. elegans*. *J. Cell Sci.* **126**, 1785–1795 (2013).
57. C. C.-H. Chen, P. J. Schweinsberg, S. Vashist, D. P. Mareiniss, E. J. Lambie, B. D. Grant, RAB-10 is required for endocytic recycling in the *Caenorhabditis elegans* intestine. *Mol. Biol. Cell* **17**, 1286–1297 (2006).
58. R. D. Klausner, J. G. Donaldson, J. Lippincott-Schwartz, Brefeldin A: Insights into the control of membrane traffic and organelle structure. *J. Cell Biol.* **116**, 1071–1080 (1992).
59. K. Sato, A. Norris, M. Sato, B. D. Grant, *C. elegans* as a model for membrane traffic. *WormBook*, 1–47 (2014).
60. K. B. Ackema, U. Sauder, J. A. Solinger, A. Spang, The ArfGEF GBF-1 is required for ER structure, secretion and endocytic transport in *C. elegans*. *PLoS ONE* **8**, e67076 (2013).
61. I. D. Zelnik, A. E. Ventura, J. L. Kim, L. C. Silva, A. H. Futerman, The role of ceramide in regulating endoplasmic reticulum function. *Biochim. Biophys. Acta Mol. Cell Biol. Lipids* **1865**, 158489 (2020).
62. G. Boncompain, A. V. Weigel, Transport and sorting in the Golgi complex: Multiple mechanisms sort diverse cargo. *Curr. Opin. Cell Biol.* **50**, 94–101 (2018).
63. T. Taguchi, K. Mukai, Innate immunity signalling and membrane trafficking. *Curr. Opin. Cell Biol.* **59**, 1–7 (2019).
64. B. M. Gardner, D. Pincus, K. Gotthardt, C. M. Gallagher, P. Walter, Endoplasmic reticulum stress sensing in the unfolded protein response. *Cold Spring Harb. Perspect. Biol.* **5**, a013169 (2013).
65. T. Lamitina, E. Chevet, To UPR... and beyond!: A new role for a BiP/GRP78 protein in the control of antimicrobial peptide expression in *C. elegans* epidermis. *Virulence* **3**, 238–240 (2012).
66. C. Couillaud, P. Fourquet, M. Pophillat, J. J. Ewbank, A UPR-independent infection-specific role for a BiP/GRP78 protein in the control of antimicrobial peptide expression in *C. elegans* epidermis. *Virulence* **3**, 299–308 (2012).
67. B. D. Grant, M. Sato, Intracellular trafficking. *WormBook*, 1–9 (2006).
68. B. Grant, D. Hirsh, Receptor-mediated endocytosis in the *Caenorhabditis elegans* oocyte. *Mol. Biol. Cell* **10**, 4311–4326 (1999).
69. M. J. Steinbaugh, S. D. Narasimhan, S. Robida-Stubbs, L. E. M. Mazzeo, J. M. Dreyfuss, J. M. Hourihan, P. Raghavan, T. N. Operaña, R. Esmailie, T. K. Blackwell, Lipid-mediated regulation of SKN-1/Nrf in response to germ cell absence. *eLife* **4**, e07836 (2015).
70. V. Singh, A. Aballay, Regulation of DAF-16-mediated innate immunity in *Caenorhabditis elegans*. *J. Biol. Chem.* **284**, 35580–35587 (2009).
71. Z. Balklava, N. D. Rathnakumar, S. Vashist, P. J. Schweinsberg, B. D. Grant, Linking gene expression in the intestine of *C. elegans* to production of gametes through the phosphate transporter PITR-1 in *Caenorhabditis elegans*. *Genetics* **204**, 153–162 (2016).
72. L. Van Rompay, C. Borghgraef, I. Beets, J. Caers, L. Temmerman, New genetic regulators question relevance of abundant yolk protein production in *C. elegans*. *Sci. Rep.* **5**, 16381 (2015).

73. T. L. Dunbar, Z. Yan, K. M. Balla, M. G. Smelkinson, E. R. Troemel, *C. elegans* detects pathogen-induced translational inhibition to activate immune signaling. *Cell Host Microbe* **11**, 375–386 (2012).
74. D. L. McEwan, N. V. Kirienko, F. M. Ausubel, Host translational inhibition by *Pseudomonas aeruginosa* Exotoxin A Triggers an immune response in *Caenorhabditis elegans*. *Cell Host Microbe* **11**, 364–374 (2012).
75. C.-Y. Kao, F. C. O. Los, D. L. Huffman, S. Wachi, N. Kloft, M. Husmann, V. Karabrahimi, J.-L. Schwartz, A. Bellier, C. Ha, Y. Sagong, H. Fan, P. Ghosh, M. Hsieh, C.-S. Hsu, L. Chen, R. V. Aroian, Global functional analyses of cellular responses to pore-forming toxins. *PLOS Pathog.* **7**, e1001314 (2011).
76. W. Rao, R. E. Isaac, J. N. Keen, An analysis of the *Caenorhabditis elegans* lipid raft proteome using gelC-MS/MS. *J. Proteomics* **74**, 242–253 (2011).
77. M. F. Perez, B. Lehner, Vitellogenins - yolk gene function and regulation in *Caenorhabditis elegans*. *Front. Physiol.* **10**, 1067 (2019).
78. H. Fares, I. Greenwald, Genetic analysis of endocytosis in *Caenorhabditis elegans*: Coelomocyte uptake defective mutants. *Genetics* **159**, 133–145 (2001).
79. A. K. Walker, F. Yang, K. Jiang, J.-Y. Ji, J. L. Watts, A. Purushotham, O. Boss, M. L. Hirsch, S. Ribich, J. J. Smith, K. Israelian, C. H. Westphal, J. T. Rodgers, T. Shioda, S. L. Elson, P. Mulligan, H. Najafi-Shoushtari, J. C. Black, J. K. Thakur, L. C. Kadyk, J. R. Whetstone, R. Mostoslavsky, P. Puigserver, X. Li, N. J. Dyson, A. C. Hart, A. M. Näär, Conserved role of SIRT1 orthologs in fasting-dependent inhibition of the lipid/cholesterol regulator SREBP. *Genes Dev.* **24**, 1403–1417 (2010).
80. A. E. Carpenter, T. R. Jones, M. R. Lamprecht, C. Clarke, I. H. Kang, O. Friman, D. A. Guertin, J. H. Chang, R. A. Lindquist, J. Moffat, P. Golland, D. M. Sabatini, CellProfiler: Image analysis software for identifying and quantifying cell phenotypes. *Genome Biol.* **7**, R100 (2006).
81. G. J. Hermann, L. K. Schroeder, C. A. Hieb, A. M. Kershner, B. M. Rabbitts, P. Fonarev, B. D. Grant, J. R. Priess, Genetic analysis of lysosomal trafficking in *Caenorhabditis elegans*. *Mol. Biol. Cell* **16**, 3273–3288 (2005).
82. A. Shaheen, Effect of the unfolded protein response on ER protein export: A potential new mechanism to relieve ER stress. *Cell Stress Chaperones* **23**, 797–806 (2018).
83. C. E. Richardson, T. Kooistra, D. H. Kim, An essential role for XBP-1 in host protection against immune activation in *C. elegans*. *Nature* **463**, 1092–1095 (2010).
84. J. J. Ewbank, O. Zugasti, *C. elegans*: Model host and tool for antimicrobial drug discovery. *Dis. Model. Mech.* **4**, 300–304 (2011).
85. M. Safra, S. Ben-Hamo, C. Kenyon, S. Henis-Korenblit, The *ire-1* ER stress-response pathway is required for normal secretory-protein metabolism in *C. elegans*. *J. Cell Sci.* **126**(Pt 18), 4136–4146 (2013).
86. E. J. Tillman, C. E. Richardson, D. J. Cattie, K. C. Reddy, N. J. Lehrbach, R. Droste, G. Ruvkun, D. H. Kim, Endoplasmic reticulum homeostasis is modulated by the forkhead transcription factor FKH-9 During Infection of *Caenorhabditis elegans*. *Genetics* **210**, 1329–1337 (2018).
87. D.-E. Jeong, Y. Lee, S. Ham, D. Lee, S. Kwon, H.-E. H. Park, S.-Y. Hwang, J.-Y. Yoo, T.-Y. Roh, S.-J. V. Lee, Inhibition of the oligosaccharyl transferase in *Caenorhabditis elegans* that compromises ER proteostasis suppresses p38-dependent protection against pathogenic bacteria. *PLOS Genet.* **16**, e1008617 (2020).
88. N. G. Bednarska, B. W. Wren, S. J. Willcocks, The importance of the glycosylation of antimicrobial peptides: Natural and synthetic approaches. *Drug Discov. Today* **22**, 919–926 (2017).
89. K. Dierking, W. Yang, H. Schulenburg, Antimicrobial effectors in the nematode *Caenorhabditis elegans*: An outgroup to the arthropoda. *Philos. Trans. R Soc. Lond. B Biol. Sci.* **371**, 20150299 (2016).
90. E. D. Nadal, G. Ammerer, F. Posas, Controlling gene expression in response to stress. *Nat. Rev. Genet.* **12**, 833–845 (2011).
91. C. E. Machamer, The Golgi complex in stress and death. *Front. Neurosci.* **9**, 421 (2015).
92. J. H. Reiling, A. J. Olive, S. Sanyal, J. E. Carette, T. R. Brummelkamp, H. L. Ploegh, M. N. Starnbach, D. M. Sabatini, A CREB3–ARF4 signalling pathway mediates the response to Golgi stress and susceptibility to pathogens. *Nat. Cell Biol.* **15**, 1473–1485 (2013).
93. J. G. Donaldson, C. L. Jackson, ARF family G proteins and their regulators: Roles in membrane transport, development and disease. *Nat. Rev. Mol. Cell Biol.* **12**, 362–375 (2011).
94. C. Riebeling, A. J. Morris, D. Shields, Phospholipase D in the Golgi apparatus. *Lipids* **1791**, 876–880 (2009).
95. M. McDermott, M. J. O. Wakelam, A. J. Morris, Phospholipase D. *Biochem. Cell Biol.* **82**, 225–253 (2004).
96. R. P. H. Huijbregts, L. Topalog, V. A. Bankaitis, Lipid metabolism and regulation of membrane trafficking. *Traffic* **1**, 195–202 (2000).
97. M. Ren, H. Feng, Y. Fu, M. Land, C. S. Rubin, Protein kinase D is an essential regulator of *C. elegans* innate immunity. *Immunity* **30**, 521–532 (2009).
98. V. Malhotra, F. Campelo, PKD regulates membrane fission to generate TGN to cell surface transport carriers. *Cold Spring Harb. Perspect. Biol.* **3**, a005280 (2011).
99. R. Medzhitov, Recognition of microorganisms and activation of the immune response. *Nature* **449**, 819–826 (2007).
100. O. Yukselen, O. Turkyilmaz, A. R. Ozturk, M. Garber, A. Kucukural, DolphinNext: A distributed data processing platform for high throughput genomics. *BMC Genomics* **21**, 310 (2020).
101. J. Singh, A. Aballay, Endoplasmic reticulum stress caused by lipoprotein accumulation suppresses immunity against bacterial pathogens and contributes to immunosenescence. *mBio* **8**, e00778-17 (2017).

**Acknowledgments:** We would like to acknowledge S.-J. Lee and S. Kwon (Korea Advanced Institute of Science and Technology) for providing the *lpin-1* RNA-seq data. In addition, G. Hermann provided the *glo-1::ssGFP* strain (GH639). We would also like to thank S.-J. Lee, E. Troemel (USD), C. Haynes (UMASS Chan School of Medicine), A. Byrne (UMASS Chan School of Medicine), and A. Munden for comments on the manuscript. We appreciate discussions with M. Walhout (UMASS Chan School of Medicine) on the nature of stress-induced genes and interactions between metabolism and gene expression. We would like to acknowledge W. Ding for technical support, C. Lewis (MIT) for metabolomics screening at the Whitehead Metabolomics core, and D. Higgins with assistance with bioinformatics. We also thank Life Science editors and S. Lall for manuscript editing. Some strains were provided by the CGC, which is funded by the NIH Office of Research Infrastructure Programs (P40 OD010440).

**Funding:** Funding to AWK was from the NIA at the NIH: R01AG053355, R56AG068670, and R01AG068670. **Author contributions:** Conceptualization: A.K.W., M.J.F., C.M.W., and L.J.S. Verification: A.K.W., M.J.F., C.M.W., and L.J.S. Formal analysis: A.K.W., M.J.F., C.M.W., L.J.S., and D.M.L. Investigation: A.K.W., M.J.F., C.M.W., L.J.S., and D.S.L. Resources: A.K.W. Data curation: A.K.W. Writing: A.K.W. Writing/editing: A.K.W., M.J.F., C.M.W., D.S.L., and L.J.S. Visualization: A.K.W. Supervision: A.K.W. Funding: A.K.W. **Competing interests:** The authors declare that they have no competing interests. **Data and materials availability:** All data needed to evaluate the conclusions in the paper are present in the paper and/or the Supplementary Materials. The GEO accession number for RNA-seq data is GSE242371.

Submitted 5 May 2023

Accepted 3 November 2023

Published 6 December 2023

10.1126/sciadv.adi5545